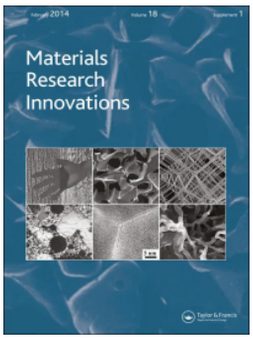

Materials Research Innovations

ISSN: 1432-8917 (Print) 1433-075X (Online) Journal homepage: www.tandfonline.com/journals/ymri20

A multifunctional nanostructured molybdenum disulphide (MoS_2): an overview on synthesis, structural features, and potential applications

C. Vidya, C. Manjunatha, A. Pranjal, I. Faraaz & K. Prashantha

To cite this article: C. Vidya, C. Manjunatha, A. Pranjal, I. Faraaz & K. Prashantha (2023) A multifunctional nanostructured molybdenum disulphide (MoS_2): an overview on synthesis, structural features, and potential applications, Materials Research Innovations, 27:3, 177-193, DOI: 10.1080/14328917.2022.2109887

To link to this article: https://doi.org/10.1080/14328917.2022.2109887

Published online: 18 Aug 2022.

MATERIALS RESEARCH INNOVATIONS
2023, VOL. 27, NO. 3, 177–193
https://doi.org/10.1080/14328917.2022.2109887

Taylor & Francis
Taylor & Francis Group

A multifunctional nanostructured molybdenum disulphide (MoS_2): an overview on synthesis, structural features, and potential applications

C. Vidya[a], C. Manjunatha[b], A. Pranjal[a], I. Faraaz[a] and K. Prashantha[c]

[a]Department of Chemical Engineering, R.V. College of Engineering, Bengaluru, India; [b]Department of Chemistry, R.V. College of Engineering, Bengaluru, India; [c]ACU-Centre for Research and Innovation, Adichunchanagiri School of Natural Sciences, Adichunchanagiri University, Karnataka, India

ABSTRACT

Molybdenum disulphide (MoS_2) is a versatile inorganic material due to its unique electronic, electrical, optical, and biological properties, hence widely studied for various engineering applications. The main objective of this review is to provide comprehensive information about MoS_2 for the researcher intended to start research on MoS_2. The beginning of the review is focused on providing information on the methods, precursors, and conditions used for the synthesis of various MoS_2 nanostructures such as nanospheres, nanotubes, nanoflakes, nanobelts, nanoflowers, nanofibers, nanoclusters, nanosheets, and nanowires. The structural features of MoS_2, both in pure and with other composite forms, are discussed in detail using the XRD, Raman, PL and UV–visible spectra reported by various research groups. Further, the detailed morphological features of both pure and composite forms of MoS_2 are also discussed by taking selected works of SEM and TEM images. Finally and very importantly, the review also summarises the multifunctional applications of the versatile MoS_2 and its composites in lubricants, exploring its tribological properties, in lithium-ion batteries, revealing its electrical and electronic property, as a catalyst for water splitting hydrogen evolution reaction, oxygen evolution reactions, endorsing its potential electrochemical property, various biomedical applications such as bio sensors, bioimaging, and very importantly in environmental applications.

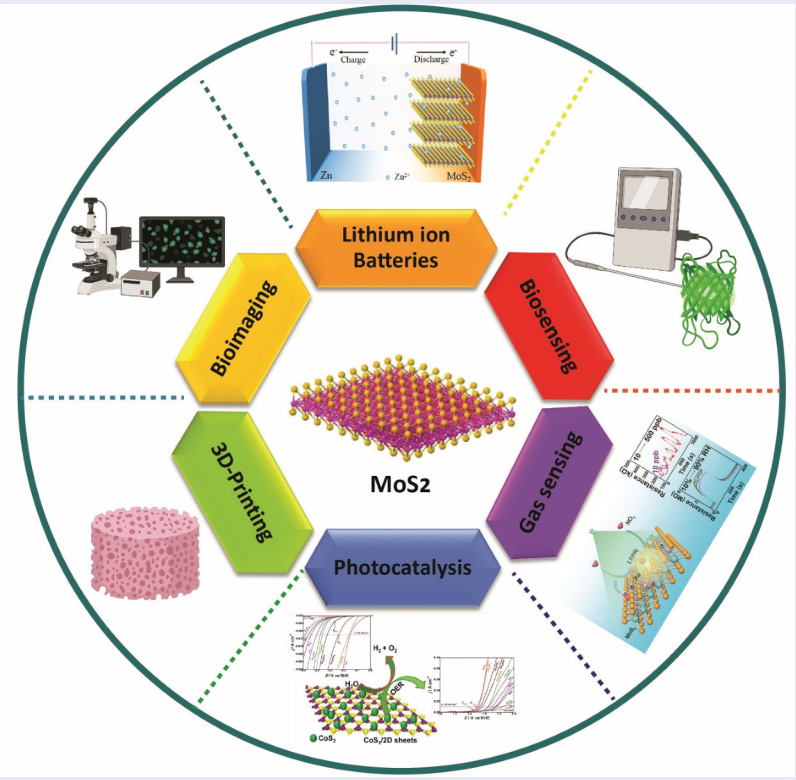

Graphical Abstract is Reproduced with permission from [1] [2], [3].

ARTICLE HISTORY
Received 04 May 2022
Accepted 01 August 2022

KEYWORDS
Molybdenum disulphide; 2D materials; water splitting; lithium-ion batteries

1. Introduction

Molybdenum disulphide is an inorganic compound made of molybdenum and sulphur with the chemical formula MoS_2. It is a silvery black solid classified as the transition metal dichalcogenide. It is a diamagnetic [4,5] indirect bandgap semiconductor [6,7]. Thin layers of molybdenum disulphide

CONTACT K. Prashantha prashantha.k@gmail.com ACU-Centre for Research and Innovation, Adichunchanagiri School of Natural Sciences, Adichunchanagiri University, BGSIT, B.G. Nagara 571448, Karnataka, India; C. Manjunatha manjunathac@rvce.edu.in Centre for Nanomaterials and Devices, Department of Chemistry, RV College of Engineering, Bengaluru 560059, India

(MoS_2) are known for their nonzero bandgap, high electrical conductivity [8–10], good thermal stability [11,12], and excellent mechanical strength [13–15]. Crystalline MoS_2 usually consists of two phases, 2 H and 3 R (H and R indicate hexahedral and rhombohedral, respectively). 1 T (T indicates the tetragonal) phase is also reported in the literature [16]. With the prevalent energy crisis, there is a need for alternate fuels to reduce the dependency on fossil fuels and other non-renewable fuel sources. Hydrogen is gaining popularity as a renewable fuel. It is a clean fuel as it produces only water vapour on combustion. One of the methods of producing hydrogen is by the electrolysis of water. The use of platinum as an electrocatalyst is common but makes the process expensive [17]. Molybdenum disulphide is found to be a possible replacement for platinum as a catalyst in electrochemical water splitting [18–21] due to its bandgap suitable for water splitting, low Gibbs free energy for hydrogen adsorption and ease of production. It is inexpensive and competent when compared to conventional catalysts. MoS_2 as an electrocatalyst finds applications in fuel cells, automobiles, electricity generation, and space travel. MoS_2 is suitable for many other applications due to its tunable bandgap, hexagonal layered structure [22], and abundance of free sulphur sites.

There are several review articles on MoS_2 which cover a number of its attributes. Many researchers have worked on its photocatalytic and electrocatalytic properties of MoS_2 along with its applications are detailed in an article by Li et al. [23]. The use of MoS_2 as electrochemical and biological sensors is reported by Sinha et al. It highlights how Transition Metal Dichalcogenides (TMDs) other than MoS_2 are suitable for sensing applications [24]. The potential use of MoS_2 as a gas sensor along with other materials is reported by Donarelli et al. [25]. Furlan et al. reviewed the lubricating properties of MoS_2 composites and tribological properties such as varied matrices, contents, processing conditions, testing temperatures, and atmospheres [26]. An article by Bazaka et al. illustrates the synthesis and applications of MoS_2 nanoparticles in the field of medicine [27]. Liu et al. highlighted the biomedical aspect of the MoS_2 nanomaterials by studying its applications, in vivo behaviour, and toxicology profiles of the material [28]. Bhattacharya et al. have depicted the dependence of optical properties on particle size. Unlike other reports, the aspect of zero-dimensional nanocrystals is highlighted [29]. The thermal properties of 2D materials are crucial for their application in electronic and optoelectronic devices. Arkadiusz and co-workers demonstrate the ways to address crucial stability issues in light-sensitive materials and can be used to understand heat management in MoS_2 and other 2D flake-based thin films [30].

Andrzej and team have investigated the temperature-dependent thermal conductivity and interfacial thermal conductance of molybdenum disulphide monolayers supported on SiO_2/Si substrates, using Raman spectroscopy. The calculated thermal conductivity (κ) and interfacial thermal conductance (g) decreased with increasing temperature from 62.2 W m^{-1} K^{-1} and 1.94 MW m^{-2} K^{-1} at 300 K to 7.45 W m^{-1} K^{-1} and 1.25 MW m^{-2} K^{-1} at 450 K, respectively [31] .

Two-dimensional (2D) MoS_2 finds its application as a catalyst or a carrier and is extensively researched because of its superior structural and electronic properties compared with those of bulk structures. Yanguang and co-workers synthesised MoS_2/RGO hybrids, which showed a greater electrocatalytic activity towards the hydrogen evolution reaction (HER) compared to other MoS_2 catalysts. A Tafel slope of ~41 mV/decade was measured for MoS_2 catalysts in the HER for the first time. This exceeds by far the activity of previous MoS_2 catalysts and results from the abundance of catalytic edge sites on the MoS_2 nanoparticles and the excellent electrical coupling to the underlying graphene network [32].

Damien and co-workers used a solvent-free intercalation method and reported chemically exfoliated MoS_2 nanosheets with a very high concentration of metallic 1 T phase proving enhanced catalytic activity towards the evolution of hydrogen with a notably low Tafel slope of 40 mV/dec. The 1 T MoS_2 also remains unaffected after oxidation, suggesting that edges of the nanosheets are not the main active sites [33].

The structural and electronic properties of MoS_2 are studied using plane wave pseudopotential method under generalised gradient approximation (GGA) scheme-based Discrete Fourier Transform (DFT) calculations. The electronic band structure and density of states calculation show many similarities between monolayer-MoS_2 and bulk-MoS_2 except the nature of the band gap which is found direct for monolayer-MoS_2 as compared to indirect for bulk-MoS_2. Tianshu et al. suggest ways to engineer the electronic properties so as to obtain direct band gap 3D layered nanoparticles or Mo doped metallic nanowires. They worked on taking the advantage of surface states to design metallic nanowires with novel catalytic and thermoelectric properties. The single sheet MoS_2 nanoparticles sized up to ~3.4 nm show no appreciable quantum confinement effects. However, their electronic structure is entirely dominated by surface states near the Fermi level. The 3D nanoparticles showed strong electronic properties on layer stacking distance, and the number of these planes and their distance can be tuned to engineer clusters with direct band gaps, at variance with the bulk [34].

In all these review papers, importance is not given to the various synthesis methods, instead the versatility of MoS_2, doped MoS_2, and its applications as electrocatalysts. This review article covers the aforementioned aspects that are missing in other review articles. It concludes with the future scope of MoS_2 and some studies, which can be performed to explore its efficiency in electrochemical water splitting.

2. Synthesis of MoS_2 nanoparticles

Molybdenum disulphide as a nanomaterial is known for a plethora of applications in lubricants [35–37], battery systems [38,39], electrochemical water splitting [18–21], biosensing [40,41], bio-imaging [42,43], environmental applications [44,45], and many more. With its ever-increasing diverse application base, various methods of synthesis have been tried and reported in the literature. These methods have led to the synthesis of various MoS_2 crystal structures and morphologies. Different articles have reported numerous morphologies such as thin films [46,47], nanowires [48–50], spheres [51], nanocrystals [52,53], Nanotubes [54], etc. Several problems such as low yield and high impurities are reported during synthesis. To overcome these, many precursors such as sodium molybdate, ammonium molybdate, thioacetamide, thiourea, and sodium sulphate are explored. Several techniques of synthesis of pure MoS_2 and MoS_2

composites reported in the literature are discussed in the following section. MoS_2 synthesis methods are summerized the Table 1.

2.1 Synthesis of pure MoS_2 nanomaterials

Synthesis of pure MoS_2 nanoparticles with varying morphologies is detailed below

2.1.1 Synthesis of MoS_2 nanotubes

Sudarson et al. reported the synthesis of MoS_2 nanotubes via a new method (horizontal reactor) and its structural elucidation and the optical properties. The MoS_2 nanotubes are polydispersed ranged between 30 and 200 nm. The MoS_2 nanotubes reported here were type II and have a strong coupling effect between optical cavity modes and the excitons [55]. Nath et al. used simple heating of trisulphide molybdenum complexes in a stream of hydrogen to synthesise Bamboo-like stacked MoS_2 [56]. Yunlei et al. synthesised MoS_2 nanotubes by hydrothermal method for potassium ion batteries and reported that the ratio of MoS_2 to the randomly produced polysulphide in the synthesised MoS_2 nanotubes is 4.29 which confirms that the synthesised MoS_2 nanotubes have quite high quality. The MoS_2 nanotubes showed superior rate capability and cyclability (127 mAh g^{-1} at 200 mA g^{-1} after 100 cycles) in the potassium ion battery [57].

Olga et al. used lead as a growth promoter for two-step synthesis of MoS_2 nanotubes. MoS_2 and Pb mixture was exposed to highly compressed shock-heated argon gas at 9900 K to get molybdenum suboxide nanowhiskers with traces of lead in the first step. The molybdenum suboxide nanowhiskers were then treated with H_2S gas at 820°C to yield MoS_2 nanotubes. The synthesis of new nanostructures from other layered materials can be best done with high-temperature shockwave system [58].

Chen et al. synthesised open-ended MoS_2 nanotubes by gas solid reaction route using ammonium molybdenum hydrate in the hydrogen atmosphere and was used as the catalyst for methanation. The MoS_2 nanotubes were added to a Ni substrate and used as catalyst for methanation reaction in a microreactor. This process offers a relatively energy-efficient method of synthesis that shows potential applications in carbon monoxide detection as well as methane generation for fuel and lighting [59] .

2.1.2 Synthesis of single-walled MoS_2 nanotubes

Remstar reported growing MoS_2 nanotubes by catalysed transport method. C60 was used as a growth promoter. It is a long reaction carried out for 22 days at a temperature of 1010 K in an evacuated silica ampoule at a pressure of 1023 Pa containing 5 wt% of C60 and MoS_2 powder. Here, C60 played the role of a catalyst, and iodine was used as a transporting agent. The reaction resulted in 15 wt% of single-walled nanotubes and the rest formed layered material. Excess C60 was removed by washing with toluene [60].

2.1.3 Synthesis of MoS_2 nanofibers and nanotubes

Zelenski and Dorhout synthesised MoS_2 nanofibers and nanotubes. A stock solution of $(NH_4)_2MoS_4$ was prepared in a solvent of choice (dimethylformamide (DMF), ethylenediamine (en), pyridine (py) (0.034 M was saturated), dimethyl sulphoxide (DMSO)). A glass frit was used to filter all the solutions to ensure the dissolution of solids in the dark red-brown solutions. The precursor solution was introduced into the thiomolybdate solution using a template piece of 5.5 mm. The solvent was dried by evaporation at 70°C on a hot plate. The loaded template was placed on a stage in a fused silica flow-through tube inside a tube furnace, which was heated to 450°C at the rate of 10°C/min. Ten per cent H_2 /N_2 atmosphere was introduced into the tube at a rate of 20 mL/min. The furnace was maintained at that condition for a period of 1 h before it was cooled to room temperature by step cooling. In the heating process, the red-brown colour of the templates laden with precursors turned black [61].

2.1.4 Synthesis of MoS_2 thin films

Barreau and Bernede demonstrated the synthesis of MoS_2 thin films using NaF (Sodium Fluoride) as an additive. It begins with the sputtering of Mo in an argon plasma. A homogeneous mixture of molybdenum, sulphur, and NaF was made by evaporating sulphur and sodium fluoride in argon plasma. The substrate temperature was increased to 823 K from room temperature. Finally, when the temperature of the substrate reached 823 K, the films were annealed, under constant argon flow, for 30 min yielding films of a 700 nm thickness [62].

2.1.5 Synthesis of discrete and dispersible MoS_2 nanocrystals

Yu et al. reported the synthesis of MoS_2 with different morphologies. Spherical, onion and tube-shaped MoS_2 nanoparticles were synthesised by reacting $Mo(CO)_6$ (molybdenum carbonyl) and TOPO (trioctylphosphine) oxide with the same precursors but varying weights of reactants, reaction time, and the reaction temperature. The detailed procedure is as follows.

Spherical MoS_2 nanoparticles were synthesised by reacting molybdenum carbonyl with elemental sulphur in trioctylphosphine oxide at a temperature between 270°C and 300°C. The synthesis involved mixing molybdenum carbonyl and trioctylphosphine oxide in a flask flushed with Argon maintained at a temperature of 250°C overnight. Sulphur/octadecene solution was rapidly injected into the system, and the temperature was gradually increased to the target value. The system was maintained at the conditions for a period of 24 to 48 h, followed by cooling to 60°C along with toluene injection into the system. The resulting dispersion was cooled to room temperature, and MoS_2 nanoparticles were isolated using anhydrous methanol in excess. Lastly, the mixture was centrifuged, and the supernatant fluid was removed [63].

In another method, the same reactants trioctylphosphine and molybdenum carbonyl of different weights were mixed in a flask flushed with argon at room temperature. Then, the flask was heated to 250°C and kept overnight. Sulphur/1-octadecene solution was rapidly injected into the system. The temperature was raised to 280°C and the system was maintained for 24 h to obtain onion and tube-shaped MoS_2 nanoparticles [63].

2.1.6 Synthesis of MoS_2 nanoflowers

Sun et al. reported a solvothermal method to synthesise flower-like MoS_2 nanoparticles. An aqueous solution of $Na_2MoO_4.2\ H_2O$ (sodium molbdate dihydrate) and $CS(NH_2)_2$ (thiourea) was mixed and stirred for 10 min. The solution was maintained at 190°C for 24 h in a 100 mL Teflon-lined

Table 1. MoS_2 synthesis methods consolidated in the form of a table.

Method	Reactants and Precursors	Reaction Conditions	Crystalline State	Morphology	Reference
Homogeneous precipitation method	$Na_2MoO_4.2H_2O$ and CH_3CSNH_2	90°C, 85°C, 82°C.	Amorphous	Ball-like morphology	[51]
Hydrothermal Synthesis	$Na_2MoO_4.2H_2O$, PVP, and NaSCN	180°C for 24 h in both stages	Hexagonal crystalline	Nano-belts	[52]
Novel supercritical ethanol route	$MoO_2(ac)_2$ and H_2S	Reactor temp. = 400°C, calcination = 800°C	Hexagonal crystalline	Aggregated nanoplates forming a sheet-like structure	[52]
Gas-Solid reaction method	$(NH_4)_2MoS_4$ and $(NH_4)_6Mo_{12}O_{39} \cdot 12H_2O$	H_2 atmosphere, 0.2 MPa for 1 h; 400°C for 10 h.	NIL	nanotubes	[59]
Gas-phase reaction method	(NH4)2MoS4 and H_2	High temperature (1200–1300 deg C)	Hexagonal crystalline	Nanotubes and nanorods	[56]
Sputtering	Mo, S, and NaF	823 K	Amorphous	Thin films	[62]
The novel chemical synthesis technique	Mo $(CO)_6$, elemental sulphur in trioctylphosphine	250°C overnight then raised to target temp (270–330°C) for 24 to 48 h.	Hexagonal or Rhombohedral	Sphere-shaped and onion or tube-shaped	[63]
Solvothermal Synthesis	$Na_2MoO_4.2H_2O$ and $CS(NH_2)_2$	190°C for 24 h	Hexagonal crystalline	Nano-flowers	[64]
Catalysed transport reaction	C60, bulk MoS_2 powders, and Iodine	1010 K for 22 days	Hexagonal Crystalline	Single-walled nanotubes	[60]
Thermal Decomposition and template-assisted growth process	$(NH_4)_2MoS_4$ DMSO and solvent of choice	Heating to 450°C at 10 deg/min increase, 10% H_2/N_2 atmosphere for 1 h	Hexagonal Crystalline	Nanofibers and Nanotubes	[61]
Inverse Micelle method	$MoCl_4$ and Na_2S	Ambient temperature and pressure conditions		Nanoclusters	[65]
Hydrothermal Synthesis	$C_4H_{14}N_2S_2.2HCl$, PVP and $Na_2MoO_4.2H_2O$		Hexagonal crystalline	Nanosheets	[66]
One-pot polyol-mediated process	Na_2MoO_4, Ethylene Glycol, and sublime Sulphur	170–190°C for 24 h	Hexagonal Crystalline	Globular	[67]
Electrochemical/Chemical Synthesis	MoO_2 nanowires	H_2S atmosphere at 800–900°C	Hexagonal Crystalline	Nanoribbons	[68]
Hydrothermal Synthesis	(1) P25 and NaOH (2) TiO_2 NPs, $Na_2MoO_4.2H_2O$ and thiourea	180°C for 24 h for both stages.	Anatase TiO_2	Nanobelts	[53]
Solution-phase method (Hydrothermal synthesis)	Graphene Oxide, Sodium Molybdate, and L-Cysteine	Annealing at 800°C for 2 h.	Hexagonal Crystalline	Layered structure	[69]
Modified Hydrothermal Method	$(NH_4)_6Mo_7O_{24} \cdot 4H_2O$, H_2NCSNH_2, surfactants 1- octanol and sodium lauryl sulphate and TiO_2	180°C for 5 h	Hexagonal Crystalline	Nano-rags	[70]
Galvanic Deposition Approach	MoO_3 powders with sulphur selenium powder mixture (50–50)	Heating to 650°C. Heating powder mixture to 300°C	Hexagonal crystalline	Monolayers of MoS_2 and $MoSe_2$	[71,72]

autoclave reactor. The black precipitate obtained was gradually cooled to room temperature, centrifuged, and dried at 50°C in a vacuum oven. The dried sample was annealed in nitrogen atmosphere at 500°C for 5 h [64].

2.1.7 Synthesis of MoS_2 nanoclusters

Wilcoxon and team synthesised MoS_2 nanoparticles using the inverse micelle method. Here, water-containing micelles become the platform for growing particles in non-aqueous media. A molybdenum halide, namely, $MoCl_4$ (molybdenum tetrachloride), and a sulfiding agent, Na_2S (Sodium sulphide), were used as precursors, which yielded particles as small as 2.5 nm. This method offers the advantage of manipulating the particle size by controlling the micelle size. This can be done by altering the emulsifier/water ratio. One disadvantage of this method is that the halides used as precursors are unstable and are not readily available. Nevertheless, it is considered one of the best techniques to synthesise semiconducting or other types of nanomaterials [65].

2.1.8 Synthesis of stable colloidal MoS_2 nanoparticles

Yang et al. synthesised MoS_2 nanoparticles by hydrothermal method for tumour therapy. Precursors used in the process were $C_4H_{14}N_2S_2.2HCl$ (cystamine dihydrochloride), PVP (polyvinylpyrrolidine), $Na_2MoO_4.2H_2O$ (sodium molybdate dihydrate). The precursors were dissolved in 40 mL of distilled water and stirred to get a homogeneous solution. The solution was transferred to a 100 mL polyphenylene lined stainless steel autoclave and heated for 12 h at a temperature of 220°C. The black product formed was washed with distilled water and centrifuged at 21,000 rpm for 10 min. The as-prepared MoS_2 NPs were stored at 4°C for further use [66].

2.1.9 Synthesis of monodispersed globular MoS_2 nanoparticles

Wang et al. reported the synthesis of globular MoS_2 nanoparticles using ethylene glycol (EG) as a precursor. Different volume ratios of water and ethylene glycol (30 mL) were taken in a PTFE (polytetrafluoroethylene) lined autoclave. This mixture was then mixed with Na_2MoO_4 (sodium molybdate), pre-processed sublimed sulphur with stirring for 2 min. This was followed by adding a trace of $MnCl_2$ (Manganese chloride) to reduce the final size of globular MoS_2 nanoparticles. The sealed autoclave was maintained at a temperature between 170°C and 190°C for 24 h in an electric drying oven. The black precipitate formed was washed with deionised water and absolute ethanol followed by centrifugation at 7000 rpm for 30 min. The product was finally dried at 60°C for 6 h [67].

2.1.10 Synthesis of nano- and micro-ribbons of polycrystalline MoS_2

MoS_2 nanoparticles and microribbons were synthesised by electrochemical or chemical method. Here, MoO_2 (molybdenum oxide) nanowires were taken as precursors and were electrically deposited on a pyrolytic graphite surface. This arrangement was then exposed to H_2S (Hydrogen sulphide) at a temperature between 800°C and 900°C to get MoS_2 [68].

2.1.11 Synthesis of MoS_2 nanoparticles using MoO_3 (molybdenum oxide) nanobelts

Zeng and Qin reported the synthesis of MoS_2 nanoparticles by a novel approach. It begins with the synthesis of MoO_3 nanobelts. The precursor solution was prepared by dissolving $Na_2MoO_4.2H_2O$ in water followed by addition of nitric acid for acidification. The solution was heated at 180°C for a period of 24 h in a stainless-steel autoclave lined with Teflon of 100 mL capacity. This resulted in the formation of a white-coloured product, which was collected via centrifugation and was washed with deionised water several times [52].

The MoO_3 nanobelts obtained were used as precursors to synthesise MoS_2 nanoparticles. MoO_3 nanobelts were dispersed in 25 mL of water followed by the addition of PVP. This mixture was stirred for 10 min to obtain a uniform suspension followed by addition of NaSCN (sodium thiocyanate) with vigorous stirring for 10 mins. The resulting mixture was transferred into Teflon-lined autoclave and heated at 180°C for a period of 24 h. The product obtained was subjected to centrifugation and thorough washing with water and ethanol. Later, the product was subjected to drying at 80°C for 12 h under vacuum to obtain the desired nanoparticles confirmed by characterisation [52].

2.1.12 Synthesis of MoS_2 nanoparticles using supercritical ethanol

Kumar, Li, and the team illustrated a synthesis technique with a very short reaction time of 10 min via a simple supercritical ethanol route for application as the anode in lithium-ion batteries [53].

MoS_2 nanoparticles were synthesised using supercritical ethanol in a SUS 316 tube reactor. A predetermined amount of water and ethanol were mixed to get a clear solution at ambient temperature. In the same solution, the desired amount of bis(acetylacetonato) dioxomolybdenum (VI) was dissolved by vigorous stirring. Aliquot was loaded into the reactor maintained at 400°C and the aliquot was immersed in a molten salt bath. After the desired reaction time, quenching of the reactor was done in a molten salt bath. The formed product was washed with distilled water and ethanol followed by drying at 70°C for 12 h. Calcination of the obtained product was carried out at 500–800°C for 5 h in 5% H_2S/Ar at a flow rate of 100 mL/min to obtain the final product [53].

2.2 Synthesis of MoS_2 nanocomposites

In this section, the synthesis of various composites of MoS_2 has been discussed.

2.2.1 Synthesis of MoS_2/graphene nanocomposites

Chang and Chen illustrated the synthesis of MoS_2 and graphene nanocomposite by the solution-phase method. The nanomaterials were synthesised using graphene oxide, sodium molybdate, and L-cysteine. L-cysteine consists of multifunctional groups such as –SH, $–NH_2$, and –COO. It can be used for conjugation with other metal ions or other functional groups [69].

2.2.2 Synthesis of MoS_2/TiO_2 nanocomposites

Hui Liu Tang and his team have reported the synthesis of TiO_2 nanoparticles decorated with MoS_2 nanoparticles to reinforce the photocatalytic activity driven by the radiation

in the visible region. The TiO_2 nanoparticles were synthesised by dissolving commercial TiO_2 in aqueous solution of NaOH by stirring for 30 min. The mixture was subjected to heating at 180°C for a period of 24 h in a 100 mL Teflon coated autoclave reactor. Later, the autoclave was gradually cooled to room temperature and the formed product was taken out. The product was washed with aqueous HCl (pH = 7), deionised water, and absolute ethanol. After washing, the product was dried at 80°C for 12 h followed by calcination at 600°C for 2 h to obtain TiO_2 nanomaterials. The next step involved the decoration of MoS_2 nanoparticles on TiO_2 nanoparticles. The TiO_2 nanobelts were mixed with sodium molybdate, thiourea, and deionised water and heated at 180°C for 24 h in a 100 mL Teflon lined autoclave reactor. After several washings with double distilled water and absolute ethanol, the heated product was dried at a temperature of 80°C for 12 h [54].

Pourabbas and Jamshidi modified the conventional hydrothermal method by reducing the heating temperature to 180°C and the duration to 5 hours which had shown an increase in the efficiency. An aqueous solution of $(NH_4)_6Mo_7O_{24} \cdot 4H_2O$ (ammonium heptamolybdate) and H_2NCSNH_2 (thiourea) was prepared in 50 mL of distilled water followed by the addition of surfactants, 1-octanol, and sodium lauryl sulphate. The contents were heated in an autoclave reactor with a Teflon lining of volume 50 mL. The product obtained was subjected to washing with ethanol and water followed by drying. The MoS_2 produced was dispersed in 300 mL of ethanol for 20 min using a high-speed homogeniser. TiO_2 was added, and the homogenisation was continued for 15 more minutes to form a suspension. The suspension thus formed was dried in a rotary evaporator to remove the solvent by evaporating at 40°C under reduced pressure. The grey precipitate formed was then collected and washed several times using distilled water and finally dried for 2 h at 60°C under vacuum [70].

2.2.3 Synthesis of MoS_2/Au heterostructures

Li and Cain showed a technique that involved depositing a film of gold (Au) of thickness 10 nm on a silicon substrate via a galvanic deposition approach. The Au film is subjected to a high-temperature annealing process, wherein the film breaks into islands and eventually forms Au nanoparticles [71].

MoO_3 (molybdenum trioxide) powder was taken in a tube furnace, and the furnace was placed in an alumina boat. The furnace was surrounded by a 50–50 mixture of sulphur and selenium powders. The furnace was heated to 650°C for 30 min and held at that temperature for 5 min. The sulphur/selenium mixture was then brought to 300°C and held there for the same time. SiO_2 membranes of thickness 20 nm were formed above the oxide-containing boat. Argon gas of extremely high assay was circulated inside the chamber to create an inert atmosphere. It also acted as a carrier gas. The process was performed at atmospheric pressure [71,72].

2.3 Additive manufacturing or 3D printing of MoS_2

Additive manufacturing of MoS_2 involves the processing of functional materials to produce products with improved functionalities. So far, additives have been applied only for 3D printing of MoS_2 for energy storage applications

Navid and his team have done a review on Progress in additive manufacturing of MoS_2 based structures for energy storage applications. Molybdenum disulphide is a well-known two-dimensional (2D) transition metal dichalcogenide with outstanding electrochemical, physical, and mechanical properties that makes it a probable entrant for energy storage electrodes via intercalation of different H+, Li+, Na+, and K + cations. The researchers determined that the processing of prominent MoS_2 based functional structures prepared by additive manufacturing processes can provide complex structures for different electrochemical applications, particularly for energy conversion/storage systems [73].

Swetha and team demonstrated the use of direct ink writing (DIW) technology to create 3D catalytic electrodes for electrochemical applications. Commercially available MoS_2 and graphene oxide powders were mixed with thixotropic, high concentration, viscous ink to yield hybrid MoS_2/graphene aerogels. A porous 3D structure of 2D graphene sheets and MoS_2particles was created after post treatment by freeze-drying and reducing graphene oxide through annealing. The 3D printed MoS_2/graphene aerogel electrodes possess an electrochemical active surface area (>1700 cm^{-2}) and were able to achieve currents over 100 mA in acidic media [74] .

Kalyan and team have fabricated an electrocatalytically active filament for fused deposition modelling (FDM) printing composed of catalytically active material, conductive fillers, and polymer. The conductive fillers like graphite, activated charcoal, and multi-walled carbon nanotubes of varying mass loading were used with the base PLA (polymer polylactic acid) to optimise a filament with good flexibility and conductivity. The 3D-printed electrodes were obtained by adding a (photo) electrocatalytically active filament into the optimised carbon/polymer filament. The researchers selected MoS2 as an archetypal 2D material to demonstrate the functionality of the 3D electrodes in energy conversion and storage applications by the modified filament. The 3D-printed MoS_2/carbon electrode showed a good (photo)electrocatalytic hydrogen evolution reaction and high capacitive performance [75].

3. Structural features of MoS_2 nanostructures

Morphology is the study of the structure of a material/substance at the subatomic level. MoS_2 is classified as a transition metal dichalcogenide (TMD), which is a part of 2D materials. A MoS_2 monolayer is generally found to have a thickness of 6.5 Å diameter. Examples of monolayer TMDs are MoS_2, WS_2, $MoSe_2$, and $MoTe_2$. These seem to have a direct bandgap making them suitable for applications in electronics. Their crystal structure indicates no inversion centre, which enables a new degree of freedom of charge carriers, namely the k-valley index. This has resulted in a new branch of physics called valleytronics. There is a strong spin-orbit coupling in TMDs leading to a spin-orbit splitting of 100 MeV in the valence band and 1–3 MeV in the conduction band.

3.1 Crystal structure of MoS_2

MoS_2 nanoparticles exist in both amorphous and crystalline forms and the same is reported frequently in the literature [76–79].

Wang et al. inferred that all the XRD peaks obtained corresponded to hexagonal MoS_2 nanoparticles (Figure 1 (a)). No diffraction peaks of impurities were found, and the lattice constant a = 3.16 A ° corresponds to the reference value of MoS_2 [76]. In another study, the crystal structure of the particle was confirmed using X-ray diffraction as peaks

observed were similar to MoS_2 having a hexagonal structure with (100) as the highest intensity indicating that the (100) plane was preferential in terms of growth [77].

On studying the XRD pattern obtained for the synthesised nanoparticles by Hu et al., four diffraction peaks were observed at (002), (100), (103), and (110) peaks [78]. Authors observed the diffraction peaks at 2θ = 14.3°, 29.0°, 32.6°, 33.5°, 35.8°, 39.5°, 44.1°, 49.7° were obtained which are analogous to the bulk MoS_2. In addition, two more diffraction peaks of copper at 43.3°, 50.4° were obtained in the copper-molybdenum sulphide hybrid (Figure 1 ()). This indicates that the copper nanoparticles were reduced on the MoS_2 nanosheet [79].

It can be inferred that the formation of the crystalline and amorphous phases of MoS_2, depends on many factors including the precursor used and the method of synthesis. Another noteworthy point is that the presence of impurities, both intentional and unintentional, can be seen as additional peaks in the diffraction pattern that aids to determine the doping possibilities of the materials.

3.2 Raman spectra of MoS_2

Jing Wuan Yu et al. conducted Raman spectroscopy at a wavelength of 632.8 nm and laser power of 1.3 mW at ambient conditions. Four first-order Raman active modes were reported. According to the literature, the peaks representing MoS_2 are 404 cm^{-1} and 379 cm^{-1} denoted by A_{1g} and E^1_{2g} respectively [80]. The Raman spectra of MoS_2 powder and nanosheets were differentiated by the additional peaks at 279 cm^{-1}, 817 cm^{-1}, and 988 cm^{-1} in the case of nanopowder and are absent in MoS_2 exfoliated nanosheets as shown in Figure 2(a). Raman spectroscopy can also be conducted with a solid-state laser of excitation wavelength 532 nm resulting in the same pattern [81].

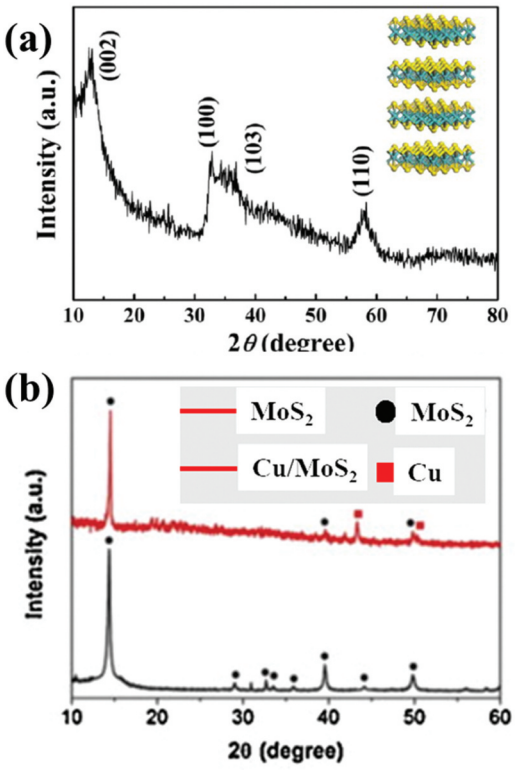

Figure 1. (a) XRD graph of hollow MoS_2 nanoparticles (Reprinted with permission from Ref [76]); (b) XRD patterns of both pure MoS_2 and hybrid made Cu-MoS_2 (Reprinted with permission from Ref [79]).

Haifeng Dong et al. synthesised hybrid materials of nitrogen-doped reduced graphene oxide (N-RGO) and MoS_2 followed by the characterisation using Raman spectroscopy at a laser excitation wavelength of 532 nm. In Figure 2(b) the characteristic peaks (E^1_{2g} and A_{1g}) of MoS_2 are visible at 375.5 cm^{-1} and 403.5 cm^{-1}, respectively. The difference between the peaks was just 27.5 cm^{-1}, which is less than pristine MoS_2, and it was inferred that the introduction of RGO could reduce the aggregation of MoS_2 nanoparticles [82].

Hong Li studied the Raman Spectra for bulk to monolayer MoS_2. The intensities or widths of the peaks vary arbitrarily, while the Raman frequencies E^1_{2g} and $A_{1g}$and the peaks vary monotonously with the layer number of ultrathin MoS_2 flakes. It is also reported that as the layer number of MoS_2 decreases, the coupling between electronic transitions and phonons become weaker which attributes to the increased electronic transition energies or elongated intralayer atomic bonds in ultrathin MoS_2. The asymmetric Raman peak at 454 cm^{-1}, is regarded as the overtone of longitudinal optical M phonons in bulk MoS_2, which is actually a combinational band involving a longitudinal acoustic mode (LA(M)) and an optical mode A_{2u}. The researchers reported a clear evolution of the coupling between electronic transition and phonon when MoS_2 is scaled down from three- to two-dimensional geometry [83].

Liangbo studied the Raman spectra of MoS_2, WS_2, and their heterostructures using density functional theory and concluded that each heterostructure configuration possesses a unique Raman spectrum in both frequency and intensity that can be explained by changes in dielectric screening and interlayer interaction. The results establish a set of guidelines for the practical experimental identification of heterostructure configurations [84].

3.3 UV–visible spectra of MoS_2

In UV–visible spectroscopy, MoS_2 shows absorption bands at 611 nm and 659 nm, and these are associated with band-edge excitations and are typical for any MoS_2 sample. Dumcenco et al. performed UV–Vis spectroscopy of monolayer MoS_2 using sapphire cuvette to ensure high optical transparency. Additional peaks were found at 430 nm and 303 nm as shown in Figure 3(a) representing van hove singularities [85].

Dipak Nimbalkar and co-workers synthesised hybrids of reduced graphene oxide (rGO) and MoS_2. Characterisation using UV–Vis spectroscopy showed that the characteristic peaks of MoS_2 at 627 and 672 nm and also the characteristic peaks of rGO in the range of 230–300 nm correspond to the p–p* plasmon peak of rGO [86]. Razi Ahmed et al. performed UV–Vis spectroscopy on three different samples – pristine MoS_2, MoS_2 exfoliated with oleylamine (OLA), and dodecanethiol (DDT). It was reported that the pristine MoS_2 showed characteristic peaks at 671 and 609 nm and the other two samples showed more or less identical peaks. In both the OLA and DDT exfoliated MoS_2, the peak at 671 nm is slightly blue-shifted to 667 and 666 nm, respectively, as shown in Figure 3(b) [87]. From all these studies, it can be inferred that typically two peaks are found in UV–Vis absorption spectra of pure MoS_2 in

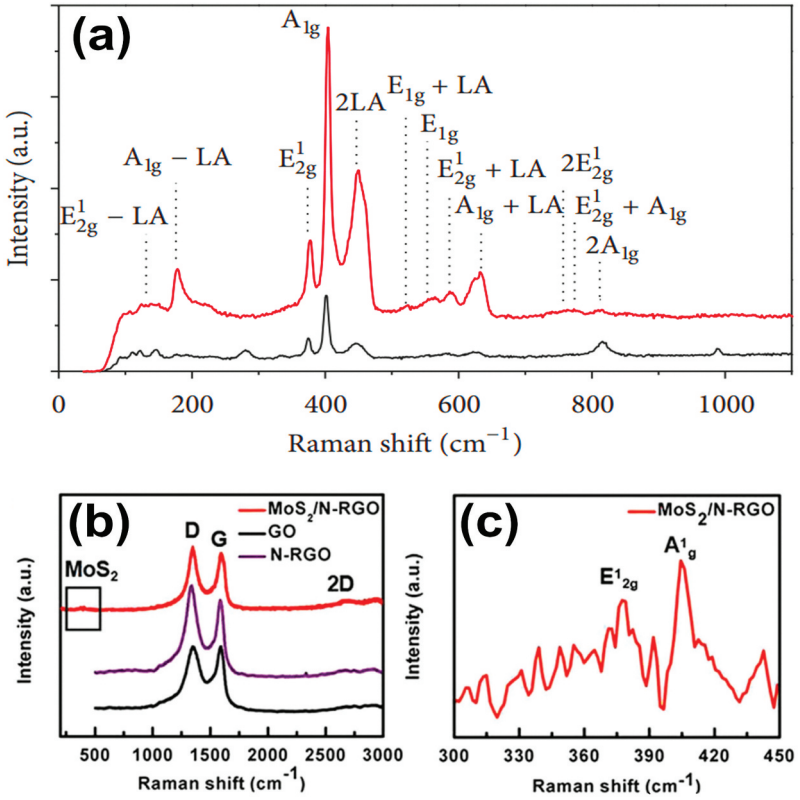

Figure 2. Raman spectra of (a) MoS_2 powder and exfoliated MoS_2 (Reprinted with permission from Ref [80]; (b) Hybrid structure of MoS_2 and N-rGO, (c) 3D MoS_2 /NRGO in the range of 300–450 cm-1. (Reprinted with permission from Ref [82]).

the range of 605–630 nm and 655–675 nm, respectively. These are the characteristic peaks of MoS_2, but additional peaks can form due to irregularities and the introduction of other composite materials.

3.4 Photo luminescence (PL) spectra of MoS_2

Xiao Li et al. reported that the PL spectra are intrinsically related to the number of layers and the thickness of the nanosheets of MoS_2 considered [88]. Zhen Li also confirmed that the photoluminescence of monolayer MoS_2 is significantly more intense than that of the bulk layer, and the introduction of layers into the monolayer decreases the intensity considerably [89]. PL spectroscopy is usually done at an excitation wavelength of 532 nm [90], and emission peaks are obtained in the range between 610 and 680 nm. Figure 4(b) represents the PL spectra of thin (~1.3 nm) and thick (~10 nm) films of annealed MoS_2. Monolayer MoS_2 has the most prominent peaks and usually, two peaks are noticed. This is the result of energy split due to valence band spin-orbital coupling. Typical peak widths are approximately 27 nm, but this may vary and get bigger for exfoliated MoS_2 nanosheets. The peak intensity of PL spectra of nanostructured MoS_2 will be higher than that of bulk MoS_2 as reported in the literature [91].

3.5 Morphology of nanoscaled MoS_2

MoS_2 nanoparticles of varying morphologies can be synthesised that offer a variety of material properties suitable for

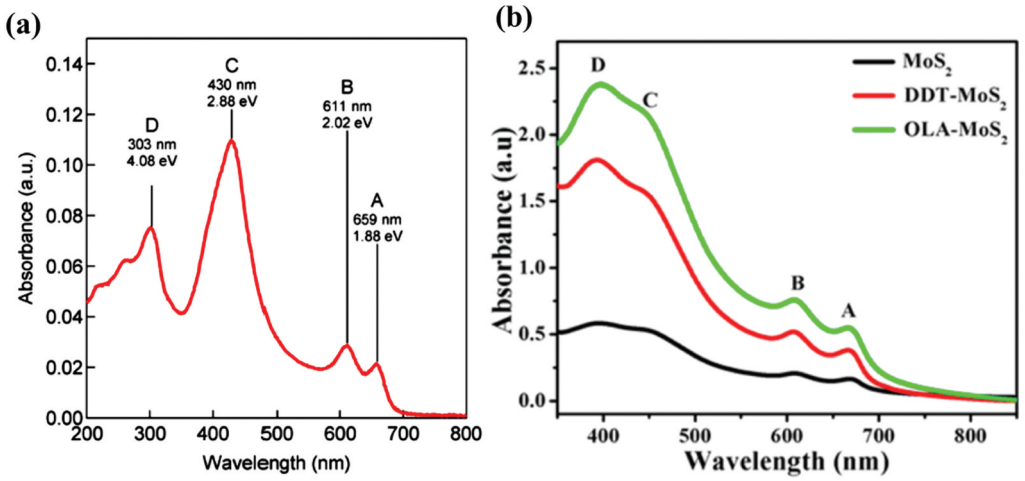

Figure 3. UV–Vis Spectra of (a) pure MoS_2 (Reprinted with permission from Ref [85]; (b) MoS_2 – pure and exfoliated with OLA and DDT (Reprinted with permission from Ref [87]).

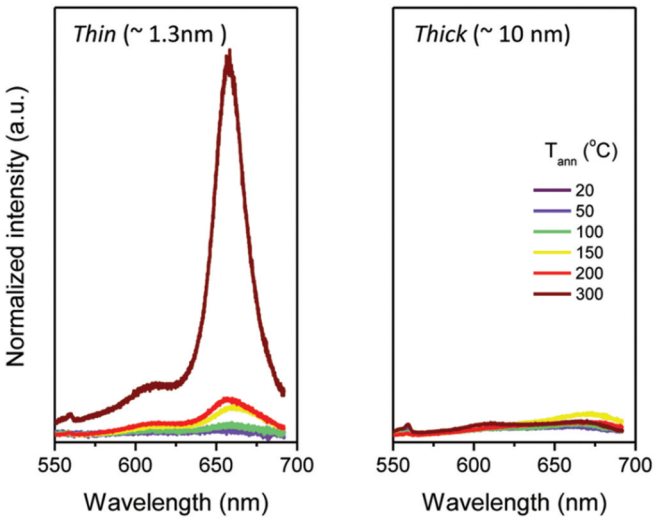

Figure 4. PL Spectra for emission wavelength with the excitation wavelength being 514 nm for thick and thin MoS_2 nanosheets (Reprinted with permission from Ref [91]).

several applications in various fields such as renewable energy, bio-sensing, bio-imaging, etc.

Zeng et al. synthesised MoO_3 nanobelts and MoS_2 nanoparticles whose FESEM images are shown in Figure 5(a,b). It was observed that the nanobelts of MoO_3 have a smooth surface and a mean width of 100–500 nm. The MoS_2 nanoparticles prepared by the same process yielded spheres with a diameter ranging from 50 to 100 nm as shown in Figure 5(c,d). MoS_2 was prepared using the MoO_3 nanoparticles as precursors, and it yielded flower-like structures as shown in Figure 5 (e,f) [52].

Heavily wrinkled morphology with a diameter in the range of 300 to 800 nm has been reported [76]. The broad size distribution can be attributed to surfactants not being added during the synthesis. Also, the surface is observed to be heavily wrinkled owing to the large surface area that enhances the electrode–electrolyte interface, making it suitable for insertion and extraction of lithium [76].

Other morphologies, such as flake-like shapes [92], nanotubes [59], and nanoflowers [64], have also been reported, and the different shapes are owing to the precursor and the method of synthesis. The morphology also depends on the form of the nanomaterial such as pure or composite.

3.6 HRTEM analysis of nanoscaled MoS_2

MoS_2 nanoparticles decorated on rGO were also verified using Transmission Electron Microscopy [93]. MoS_2 nanoparticles were lying flat on the RGO, which was observed by the light contrast of the TEM image (Figure 6(a,b)) [94].

TEM images depict hollow interiors of the particle (Figure 6(c)), which is following the SEM images and selected area electron diffraction is also seen in (Figure 6(d)) from all images it can be concluded from the images is that the particles are made of nanosheets [94].

(Figure 6(e,f)) show copper nanoparticles successfully decorated on MoS_2 sheets covering a very large area with the particles ranging from 1 to 5 nm, this can be attributed to coordination between sulphur atoms of MoS_2 and copper ions before reduction [79]. In another report, AFM images reveal the thickness of three layered nanosheets as 3.5 nm resulting in the thickness of a single layer in the range of 0.9–1.2 nm [79].

4. Multi-functionality of MoS_2 nanostructures

MoS_2 has a lot of favourable characteristics like high electrical conductivity, tunable band-gap, and excellent mechanical properties like sliding layers making it suitable for a wide range of applications discussed in the following subsections.

4.1 Lubricants and grease additives

The dense hexagonal lamellar structure of MoS_2 shows stacked layers of S-Mo-S held by weak van der Waals forces, which means that the layers can slide over one another easily and therefore MoS_2 can be used in lubricants [95]. It is mostly used as a lubricating additive in oils and paraffin due to its excellent anti-wear and friction-reducing

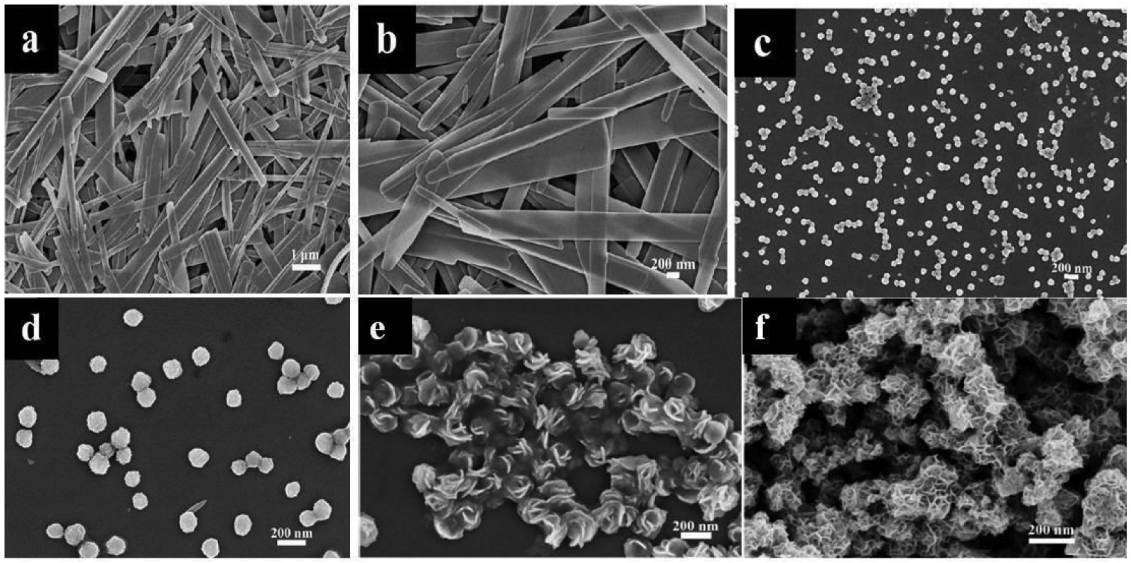

Figure 5. FESEM Images of (a, b) MoO_3 nanobelts; (c, d) and MoS_2 nanoparticles (Reprinted with permission from Ref [52]; FESEM Images of MoS_2 nano-flowers made by MoO_3 nanobelts where (e) NaSCN is directly added; (f) and further HCl is added (Reprinted with permission from Ref [52].

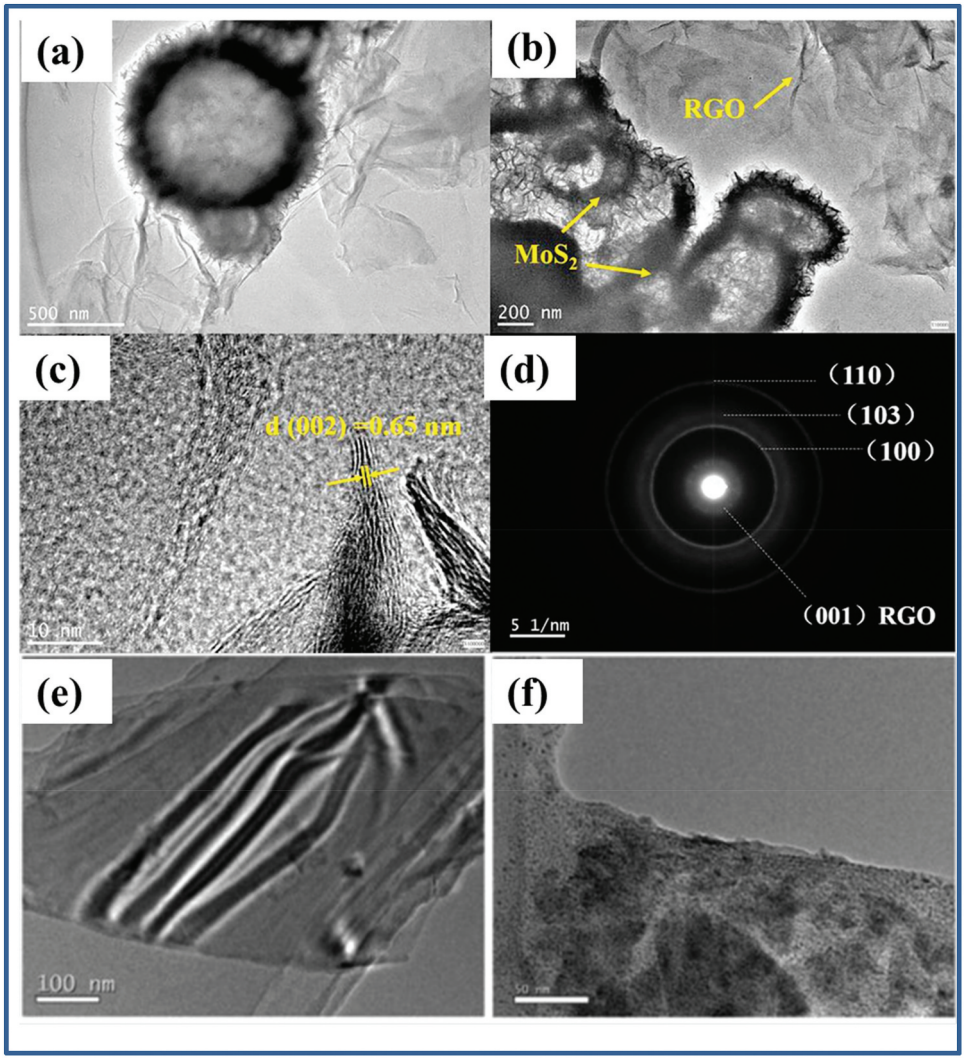

Figure 6. (a) TEM image of MoS_2 nanoparticles decorated on rGO; (b) HRTEM of MoS_2 nanoparticles decorated on rGO; (c) TEM image of hollow MoS_2 nanoparticles (d) Selected area diffraction (Reprinted with permission from Ref [94]); (e) TEM images of MoS_2 nanosheet (f) TEM images of Cu-MoS_2 hybrid Reprinted with permission from Ref [79]).

properties along with the ability to withstand extreme pressures. Hu and team reported that nano-sized MoS_2 usually has better tribological applications than bulk MoS_2 in both friction reduction and wear resistance [96]. In nano-sized MoS_2, studies have been done on identifying the best possible morphology for lubricants.

Hu et al. reported that MoS_2 nanoballs have better tribological properties than MoS_2 nano-slices at an additive concentration of 1.5 wt% [96]. However, these results are contradictory. Vattikuti and co-workers compared the efficiencies of nanoballs and nanosheets, and they reported that the MoS_2 nanosheets adhere better on the metal surface being lubricated and reduce friction more than nanoballs. They reported 0.1 wt% to be the optimal concentration of MoS_2 to be added as an additive to lubricating oils [97]. In studies undertaken by Kogovsek and Kalin, the size and morphology of MoS_2 did not sufficiently alter the coefficient of friction when compared to the actual material being utilised [98]. Figure 7 shows an example of a tribological test that can be employed to test the lubricant properties of MoS_2 nanoballs [96].

To determine the best suitable morphology of MoS_2 for tribological applications, Meirong Yi and the team performed a study where they synthesised three different morphologies including nano-flowers, nanospheres, and nanosheets [99]. They reported that the best tribological application was obtained with nanosheets, which showed a 41.1% reduction in friction coefficient and 76.8% reduction in wear.

Researchers have explored the possibility of enhancing lubrication by using composites of MoS_2 with other materials. Reduced graphene oxide (RGO)/MoS_2 nanocomposites, in comparison with pure MoS_2, show improved stability, dispensability in oil, and enhanced lubricating ability in vacuum environments [93]. Other applications of MoS_2 as a lubricant additive include the usage in the steering linkages, ball joints, wheel bearings, construction, mining, and agricultural equipment. In the military, MoS_2 can be used to grease many of the joints found in weapons and missile launchers. MoS_2 is also used in solid film lubricants where it can provide sliding and low wear without the use of any liquid lubricant [100]. It is also suitable for aerospace applications because of its good lubricating ability in a vacuum and under high loads [101].

4.2 Lithium-ion batteries

Lithium-ion batteries (LIBs) are streamlined energy storage devices that are widely used because of their high

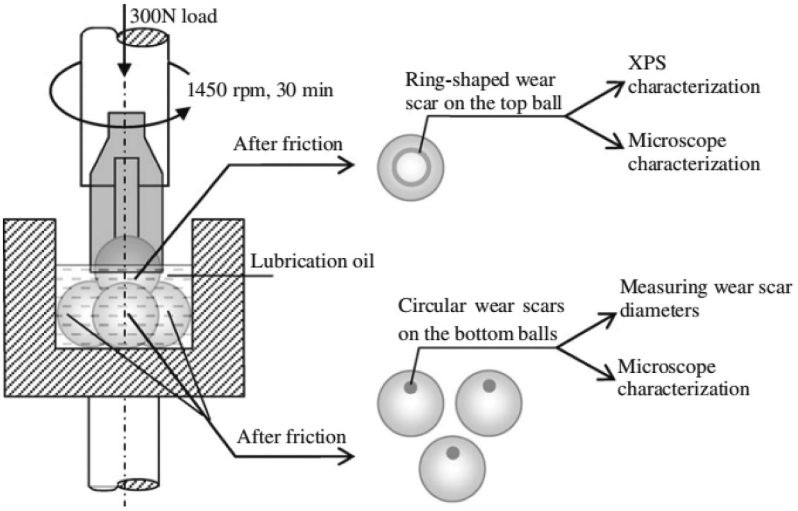

Figure 7. Schematic of a tribological test used to check the lubricating properties of MoS_2 nanoparticles. (Reprinted with permission from Ref [96]).

energy density, long cycling, and rate capability. The most prevalent material used to prepare anodes in lithium-ion batteries is commercial graphite. However, due to its low specific capacity, researchers have been studying potential alternatives for lithiated graphite. The unique structure of MoS_2 means that foreign particles can easily intercalate and decalate inside the structure. The interlayer spacing between the S-Mo-S layers at 0.615 nm is much more than graphite, which is 0.335 nm, and this extra spacing implies that lithium ions can easily enter the anode without damaging the material. This leads to a higher theoretical capacity of anodes made with MoS_2 [102]. Figure 8 shows the different molecular mechanisms of how lithium can get intercalated within the structure of MoS_2. All intercalated Li ions along the b-axis are pushed towards the interior of the crystal. In this example, a row of four intercalated Li ions takes in an incoming Li ion, making the row with five ions [103].

Chang et al. synthesised graphene-like MoS_2/amorphous carbon (a-C) composites. The graphene-like MoS_2 nanosheets were uniformly dispersed in amorphous carbon, and MoS_2/a-C composites exhibited high capacity and excellent cyclic stability when used as anode materials for Li-ion batteries. The composite prepared by adding 1.0 g of glucose in hydrothermal solution exhibited the highest reversible capacity (962 $mAhg^{-1}$) and excellent cyclic stability [104]. Another similar study, Wang Shiquan et al. also synthesised MoS_2 nanoflakes for lithium-ion battery applications; they reported that MoS_2 electrodes prepared can store lithium reversibly in a voltage range of 0.01–3 V and shows good cycling ability [105]. These studies show that nanoflakes have high potential in lithium-ion batteries. There are specific uses of MoS_2 quantum dots (QDs) in lithium-ion battery applica-

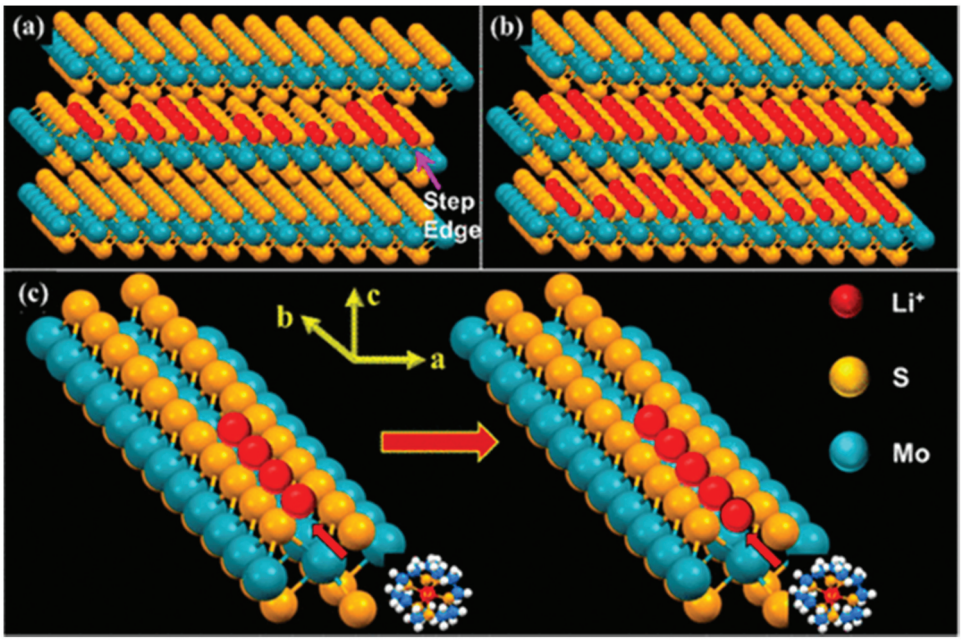

Figure 8. Illustrative depiction of the Li-ion intercalation of MoS2 along the b-axis. The first layer underneath the selvedge is intercalated first to (near) completion prior to the intercalation of the second layer (a, b). A solvated Li ion is initially intercalated at the step (c). All intercalated Li ions along the b-axis are pushed towards the interior of the crystal. In this example, a row of four intercalated Li ions takes in an incoming Li ion, making the row with five ions. (Reprinted with permission from Ref [103]).

tions. Spinel $Li_4Ti_5O_{12}$ (lithium titanate oxide) is an alternative material that is used as an anode in lithium-ion batteries because of its stability and zero strain nature, but the main limitation of this material is the fast fading of its capacity and poor rate performance. $Li_4Ti_5O_{12}$ nanosheets anchored with MoS_2 QDs exhibit exceptional lithium storage capacity along with high cycling ability and high specific capacity. This is because of the strong hetero-interfacial effect observed between the nanosheets and MoS_2 QDs [102].

It can be seen that MoS_2 has a very good potential to replace graphene in lithium-ion battery applications because of the very good ability to intercalate lithium ions into its structure. This is helped by the increased spacing between the layers when compared to graphene.

4.3 Catalysts in water-splitting

Water-splitting is the process in which water is split into its components of Oxygen and Hydrogen. This process has two main reactions: HER (Hydrogen Evolution Reaction) and OER (Oxygen Evolution Reaction). This process aids in Hydrogen collection and storage. This requires a suitable catalyst because of the high energy required by the reaction, and the use of a catalyst generally makes the process easier. The catalyst is generally Platinum, but Platinum cannot be used as it is expensive and though it has great HER, it has poor OER. So, molybdenum disulphide has been proposed as an alternative to platinum.

An ideal catalyst for such applications must have a large current density, low over potential, a small Tafel slope, and good stability in all conditions. The tunable bandgap and versatile nature of MoS_2 means researchers have considered it as a feasible material for catalytic applications [101]. Bulk MoS_2 has a smaller band gap of 1.3 eV, and as it starts losing layers the bandgap keeps increasing until monolayer MoS_2 has 1.9 eV, this is what is meant by a tunable bandgap [105]. This implies that in photochemical water splitting a wide variety of light spectrum can be harvested. Initially, bulk MoS_2 exhibited low catalytic activity because of limited active sites, but a lot of work has been done on improving the surface characteristics, composition, and using MoS_2 in conjunction with other materials like graphene oxide or TiO_2 to improve the catalytic activity [106].

Studies have shown that nanosheets or nanoparticles of MoS_2 have better electrochemical catalytic activity because of increased active sites and lower Tafel slopes but even then MoS_2 does not show good activity in OER when compared and this is the reason for conjugating it with other materials like CdS or TiO_2. Such conjugation can be considered as a viable route towards the manufacture of an excellent catalyst based on MoS_2. Ying Liu and team constructed a MoS_2 /CdS heterostructure and tested its efficiency in water splitting, and they reported that usage of MoS_2 extends the utilisation of visible light and reduces the breakdown of CdS in working conditions. So, this hetero-junction of MoS_2 and CdS shows great potential in the application of photochemical water splitting [107].

4.4 Bio-sensors

Molybdenum disulphide shows good sensing properties because of its semiconducting nature, it can be used to manufacture FETs, and also two-dimensional materials possess high surface area; they make very good candidates for gas sensing applications. MoS_2 based sensors are usually FETs that use pure or functionalised MoS_2 nanosheets which act as a dielectric layer. This layer specifically captures the molecule that is being targeted and signals the presence of that particular molecule [108]. Figure 9 shows a sensor using MoS_2 to identify target molecules; it is supported on a block of Si/SiO_2 [109].

This application of MoS_2 is mostly used to create sensors with environmental uses. Mercury ions have an affinity with sulphur, MoS_2 has free sulphur sites, and therefore Hg^{2+} ions can be adsorbed onto the surface of MoS_2 FETs and lead to the detection and removal of mercury ions in an environment [108]. Kangho Lee and the team synthesised MoS_2 thin films and used them in the sensing of ammonia (NH_3). They reported that manufactured sensors show fast response time towards NH_3 but do not recover immediately at room temperature. Nevertheless, they concluded that sensors made with MoS_2 are viable sensors for mass production [110].

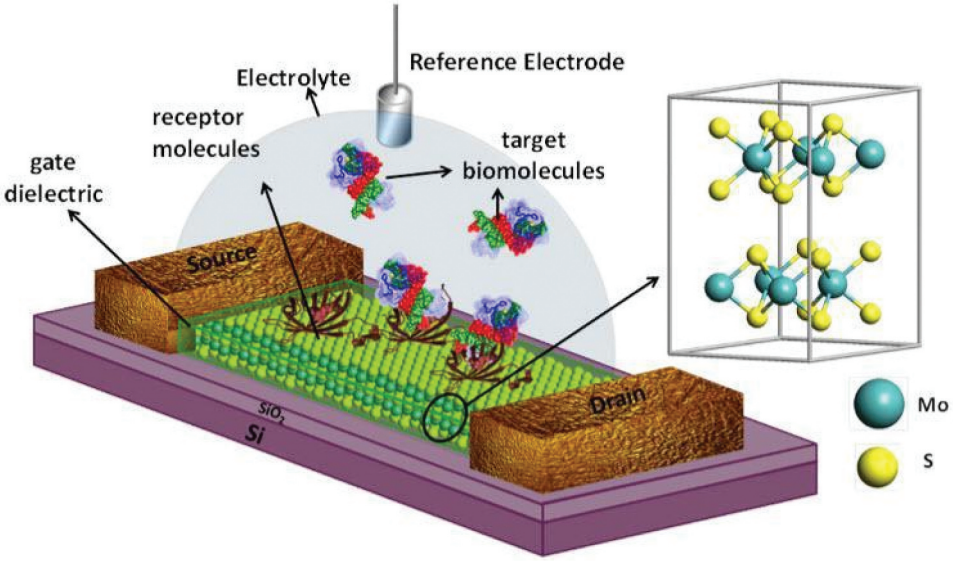

Figure 9. Depiction of MoS_2 as a sensor being supported on a SiO_2/Si structure. (Reprinted with permission from Ref [116]).

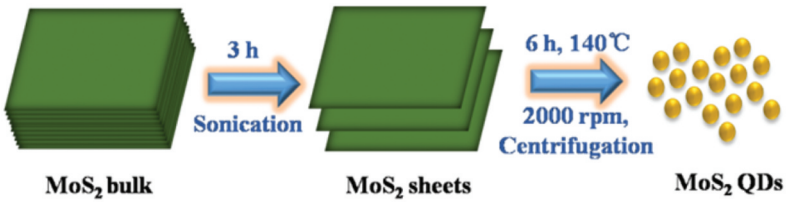

Figure 10. Flow diagram of the synthesis of MoS_2 QDs (Reprinted with permission from Ref [115]).

The well-explored gas sensing application of MoS_2 is the sensing of NO (nitric oxide). NO is electron-withdrawing and therefore it gets adsorbed onto the surface of MoS_2 nanosheets reducing the resistance and therefore increasing the current which is detected by the sensor [108]. Hai Li and team successfully reported that single and multilayer MoS_2 nanosheets have been used to detect NO gas with single-layer sheets being more efficient [111]. MoS_2 has also been used to manufacture sensors for detecting humidity [112], volatile organic contaminants [108], and doxycycline [113].

4.5 Bioimaging

Bioimaging is the tracing of live cells with the use of fluorescent probes, and it is a non-invasive process of visualising the processes occurring in the body and the cells that undertake them. Since the human body very quickly expels any foreign object, the retention of any probe is an important factor in the design of such probes. Transition metal QDs have been explored, but recently MoS_2 has come into the spotlight because of its favourable characteristics. MoS_2 molecules are negatively charged and can easily be dispersed in biofluids and since they have free sulphur sites, they can easily combine with thiol species like amino acids and travel through the living body [102]. This functionality can be further helped by the synthesis of biocompatible MoS_2 QDs using methods like sodium intercalation. The probes produced by this method are found to be nearly non-cytotoxic even at higher concentrations.

Qingqing Liu and team manufactured highly biocompatible MoS_2 QDs with excellent water solubility and reported that due to their remarkable optical properties they can directly be used in vitro imaging. They reported that alkaline solution is the key to forming such materials [114]. Yin et al. reported that MoS2 QDs were prepared by a simple solvothermal method in N-methyl-2-pyrrolidone (NMP), as shown in Figure 10. The prepared products were centrifuged for several minutes. Afterwords, the transparent light yellow solution was obtained. To remove the solvent, the obtained solution was evaporated under vacuum at a certain temperature. Then, the obtained precipitate was redispersed in ethyl acetate to acquire the MoS2 QD powder by filtration and followed by vacuum volatilisation. Figure 10 shows the flow diagram of this particular synthesis technique.

Recently, Jaiswal et al. developed a methodology targeted at the utilisation of sacrificial amine donors for C–H functionalization with MoS2 quantum dots (QDs) as the catalyst as well as the photosensitiser [116]. Since MoS_2 is considered non-toxic and can easily travel through the human body, it can be used to synthesise extremely versatile bio-imaging particles. Due to its optical properties, it can also be tracked within the body using in-vitro imaging directly.

4.6 Environmental applications

Given molybdenum disulphide's unique properties stemming from the free sulphur sites that appear in large quantities on the surface, this free sulphur can attract other metal ions and get them adsorbed onto them and help in the removal of such heavy metals from water. Bulk MoS_2 does not work efficiently in this application because of its smaller interlayer spacing compared to other adsorbents, but nano-sized MoS_2 works efficiently and lots of structures and morphologies have been explored for the same. Heavy metals like mercury and cadmium are easily adsorbed onto the surface of MoS_2, this is also because of the strong Lewis acid–base interactions [108]. Chang Liu et al. reported that 2D molybdenum disulphide nanosheets can also be used to capture lead (Pb^{2+}) ions with fast adsorption rates [117]. They attributed this to the complexation between lead and free sulphur sites on the surface as well as the affinity between the positively charged Pb and negatively charged MoS_2 sites. Apart from these, MoS_2 can also be used to adsorb zinc, cobalt, and other heavy metals. Figure 11 shows the interaction between lead and MoS_2 monolayers. Due to specific interactions between the heavy metals, MoS_2 adsorbents are selective, and depending on the concentration and composition of heavy metals in a given sample of water, they will adsorb in the order Hg > Pb > Cd > Zn [108].

Molybdenum disulphide can also be used as an adsorbent for organic materials like dyes, oils, and antibiotics [118,119]. When compared to adsorption of heavy metals where adsorption takes place due to affinity between heavy metals and sulphur sites, here it is because of the hydrophobic nature. The adsorption capacity of the prepared structure depends on the surface area; therefore, it must be a priority to increase the surface area and minimise the restacking of layers onto themselves.

Lastly, one of the miscellaneous properties of molybdenum disulphide is that it displays antimicrobial activity against E. coli and other bacteria. The exact mechanism of this antimicrobial ability has not been completely detailed, but there are a few theories that include membrane damage by sharp edges of the MoS_2 structure and peroxidase catalyst activity [108].

Research can be done on understanding the antimicrobial activities of MoS_2 better and applying them in real-life situations. There are lots of other contaminants in the environment in which MoS_2 can be used for removal and further work on identifying such contaminants and manufacturing suitable structures of MoS_2 for such removal can be done.

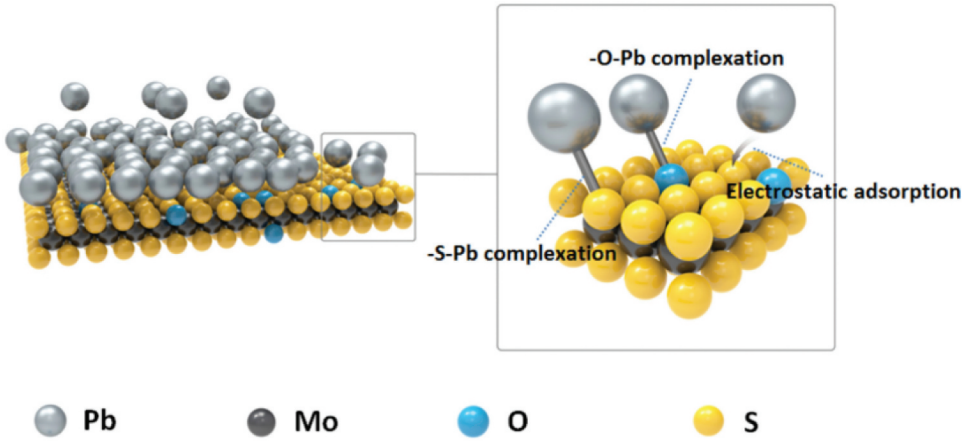

Figure 11. Diagrammatic illustration of the mechanism of removal of lead from wastewater with the use of a MoS2 monolayer (Reprinted with permission from Ref [117]).

5. Conclusion

To summarise, the MoS_2 is proved to be a very versatile material due to its various multifunctional properties as revealed by various research works. The research work confirms that the structural morphologies of MoS_2 can be effectively tuned by applying various synthesis approaches, reaction conditions, and precursors. It is very flexible in the techniques of synthesis, which are also feasible on the laboratory scale. Further, its electronic, optical, chemical, and catalytic properties can be tailored by making it a composite with RGO, CNT, metallic nanoparticles, metal oxides, etc. Further, the pure and composite forms of MoS_2 exhibit multifunctional applications in various fields such as optoelectronics, tribology, bio-sensing, bio-imaging, in vitro imaging, and photoelectrocatalysis. It holds a lot of potential in the field of renewable energy, particularly hydrogen generation. MoS_2 has a very good potential to explore and also to further enhance its performance in various applications by doping, surface functionalization with biomolecules, polymers, nanometals, etc.

Disclosure statement

No potential conflict of interest was reported by the author(s).

Notes on contributors

Vidya C working as Assistant Professor in Department of Chemical Engineering, Rashtriya Vidyalaya College of Engineering, Bengaluru, Karnataka, India. She is highly self-motivated researcher demonstrated research expertise in green synthesis of nanomaterials, effluent treatment, nanocomposites, and semiconductors. She is a regular reviewer for International journals and has published research papers in peer-reviewed international journals.

Manjunatha C currently working as an Assistant professor in the Department of Chemistry, RV College of Engineering, Bengaluru, INDIA. He obtained M.Sc in Inorganic Chemistry from Department of Chemistry, Central College Campus, Bangalore University in 2004 and Ph.D in Faculty of Science-Applied Chemistry, from VTU in 2013 from VTU. He has 16 years of teaching experience and 12 years of research experience. He is guiding 2 PhD, guided 35+ UG and PG projects and has published over 40+ peer reviewed journal articles. He has written 3 book chapters published in Elsevier and Springer publications. He has h-index of 10 with 350 citations. He is also serving as member of Editorial board for the "ECS Sensor Plus" (IOP Publishing) and "Applied Research" (Wiley). His research interests include inorganic nanomaterials chemistry, surface and colloidal chemistry and electrochemistry, with a focus on the design and synthesis of differently shaped functional inorganic materials and their applications in energy storage and conversion, photocatalysis, water purification, phosphors, sensors and nanomedicine.

Pranjal completed his Bachelors in Chemical Engineering from R. V. College of Engineering in 2020. During this time, he had worked on several projects like manufacture of MoS2 nanoparticles for catalysis applications using novel methods. He is a proactive researcher in the field of nanotechnology, who is currently working in Unilever with the Global Design Centre team as a research and development associate in the Home Care division. He is working on developing laundry detergent powders across various geographies of the world.

Faraaz is currently working at Unilever Industries Private Limited as a Research executive in the Global Design centre for Surface Cleaners in the Home and Hygiene department. At Unilever he has worked on multiple formats like creams, gels and sprays over the last 2 years and helped in bringing to market some key Cif brand products. He joined Unilever in 2020 after completing his bachelors in Chemical Engineering at RV college of engineering. During his bachelors, he has worked on several projects like manufacturing MoS2 nanoparticles for sensor applications using novel methods, also completing an internship at Sami Labs. Faraaz is a self-motivated researcher with interests in nanomaterials, product design and material sciences.

Prof. Prashantha Kalappa is a Professor and Dean, Faculty of Natural Sciences at Adichunchanagiri University, Mandya District, India. Before moving to India, he was a Professor at the Polymers and Composites Technology & Mechanical Engineering Department, Institut Mines-Télécom, Lille-Douai, France (Formerly known as Ecole Nationale Supérieure des Mines de Douai, France). He has also served as Dean for International Scientific affairs in the same institute. Prof. Prashantha's research mainly focuses on Advanced Nanomaterials, Biopolymers, Nanocomposites and Blends their Synthesis, Processing, 3D Printing, Rheology, Morphology and Structure-Property Relationships. Prof. Prashantha has worked as a Post-Doctoral Fellow at the Department of Materials Science and Engineering, Indian Institute of Science (IISc), Bengaluru, India from 2002-2003. Then worked as a KOSEF Post-Doctoral Fellow at Chonbuk National University, South Korea, He is a regular reviewer for many International journals and he has published 85 research papers in peer-reviewed international journals with over 3500 citations with h-index of 27. Enlisted in Elsevier BV's new list of the top 2% Scientists in the World for 2021. He has successfully completed national and regional projects, programs with industries and European Projects (Horizon 2020 and Interreg). He has successfully supervised 5 PhD and more than 25 MS students. Has visited more than 40 countries and delivered many key note and invited lectures at International conferences.

ORCID

C. Manjunatha http://orcid.org/0000-0003-0422-9614
K. Prashantha http://orcid.org/0000-0001-8350-3970

References

[1] Chen P, Hu J, Yin M, Bai W, Chen X and Zhang Y. (2021). MoS 2 Nanoflowers Decorated with Au Nanoparticles for Visible-Light-Enhanced Gas Sensing MoS2 Nanoflowers Decorated with Au Nanoparticles for Visible-Light-Enhanced Gas Sensing. ACS Appl. Nano Mater., 4(6), 5981–5991. 10.1021/acsanm.1c0084710.1021/acsanm.1c00847.s001

[2] Borthakur P, Boruah P K, Das M R, Ibrahim M M, Altalhi T, El-Sheshtawy H S, Szunerits S, Boukherroub R and Amin M A. (2021). CoS 2 Nanoparticles Supported on rGO, g-C 3 N 4 , BCN, MoS 2 , and WS 2 Two-Dimensional Nanosheets with Excellent Electrocatalytic Performance for Overall Water Splitting: Electrochemical Studies and DFT Calculations CoS2 Nanoparticles Supported on rGO, gC3N4, BCN, MoS2, and WS2 Two-Dimensional Nanosheets with Excellent Electrocatalytic Performance for Overall Water Splitting: Electrochemical Studies and DFT Calculations. ACS Appl. Energy Mater., 4(2), 1269–1285. 10.1021/acsaem.0c0250910.1021/acsaem.0c02509.s001

[3] Li H, Yang Q, Mo F, Liang G, Liu Z, Tang Z, Ma L, Liu J, Shi Z and Zhi C. (2019). MoS2 nanosheets with expanded interlayer spacing for rechargeable aqueous Zn-ion batteries. Energy Storage Materials, 19 94–101. 10.1016/j.ensm.2018.10.005

[4] Chen Q, Su K, Zhang M. Structure, thermal, magnetic and magneto-optical properties of core/shell Fe3O4@MoS2 doped diamagnetic glasses. J Non-Crystalline Solids. 2019;511:166–176.

[5] Sanikop R, Sudakar C. Tailoring magnetically active defect sites in MoS 2 nanosheets for spintronics applications. ACS Appl Nano Mater. 2020;3(1):576–587.

[6] Hu L, Song X-F, Zhang S-L, et al. MoS2 nanoparticles coupled to SnS2 nanosheets: the structural and electronic modulation for synergetic electrocatalytic hydrogen evolution. J Catal. 2018;366:8–15.

[7] Ma C, Yan J, Huang Y, et al. Direct–indirect bandgap transition in monolayer MoS 2 induced by an individual Si nanoparticle. Nanotechnology. 2019;31(6):065204.

[8] Hamid M, Usman M, Zubair T, et al. Shape effects of MoS2 nanoparticles on rotating flow of nanofluid along a stretching surface with variable thermal conductivity: a Galerkin approach. Int J Heat Mass Transfer. 2018;124:706–714.

[9] Ren J, Ren R-P, Lv Y-K. A flexible 3D graphene@CNT@MoS2 hybrid foam anode for high-performance lithium-ion battery. Chem Eng J. 2018;353:419–424.

[10] Wang G, Zhang J, Yang S, et al. Vertically aligned MoS 2 nanosheets patterned on electrochemically exfoliated graphene for high-performance lithium and sodium storage. Adv Energy Mater. 2018;8(8):1702254.

[11] Malkappa K, Ray SS, Kumar N. Enhanced thermo-mechanical stiffness, thermal stability, and fire retardant performance of surface-modified 2D Mo 2 nanosheet-reinforced polyurethane composites. Macromol Mater Eng. 2019;304(1):1800562.

[12] Zhang W, Zhang X, Wu H, et al. Impact of morphology and dielectric property on the microwave absorbing performance of MoS2-based materials. J Alloys Compd. 2018;751:34–42.

[13] Wang H, Jiang H, Hu Y, et al. Interface engineering of few-layered MoS2 nanosheets with ultrafine TiO2 nanoparticles for ultrastable Li-ion batteries. Chem Eng J. 2018;345:320–326.

[14] Xia Y, He Y, Chen C, et al. MoS2 nanosheets modified SiO2 to enhance the anticorrosive and mechanical performance of epoxy coating. Prog Org Coat. 2019;132:316–327.

[15] Madeshwaran SR, Jayaganthan R, Velmurugan R, et al., Mechanical and thermal properties of MoS2 reinforced epoxy nanocomposites, Journal of Physics: Conference Series, 991 2018 012054.

[16] Lei Z, Zhan J, Tang L, et al. Recent development of metallic (1T) phase of molybdenum disulfide for energy conversion and storage. Adv Energy Mater. 2018;8(19):1703482.

[17] Benson J, Li M, Wang S, et al. Electrocatalytic hydrogen evolution reaction on edges of a few layer molybdenum disulfide nanodots. ACS Appl Mater Interfaces. 2015;7(25):14113–14122.

[18] Xiong Q, Wang Y, Liu P-F, et al. Cobalt covalent doping in MoS 2 to induce bifunctionality of overall water splitting. Adv Mater. 2018;30(29):1801450.

[19] Zhu Y, Song L, Song N, et al. Bifunctional and efficient CoS 2 – C@MoS 2 core–shell nanofiber electrocatalyst for water splitting. ACS Sustain Chem Eng. 2019;7(3):2899–2905.

[20] Guo Y, Park T, Yi JW, et al. Nanoarchitectonics for transition-metal-sulfide-based electrocatalysts for water splitting. Adv Mater. 2019;31(17):1807134.

[21] Huang Y, Liu L, Liu X. Modulated electrochemical oxygen evolution catalyzed by MoS 2 nanoflakes from atomic layer deposition. Nanotechnology. 2019;30(9):095402.

[22] Vazirisereshk MR, Martini A, Strubbe D, et al. Solid lubrication with MoS 2: a review. Lubricants. 2019;7(7):57.

[23] Li Z, Meng X, Zhang Z. Recent development on MoS2-based photocatalysis: a review. J Photochem Photobiol C Photochem Rev. 2018;35:39–55.

[24] Sinha A, Dhanjai BT, Huang Y, et al. MoS2 nanostructures for electrochemical sensing of multidisciplinary targets: a review. Trends Analyt Chem. 2018;102:75–90.

[25] Donarelli M, Ottaviano L. 2D materials for gas sensing applications: a review on graphene oxide, MoS_2, WS_2 and phosphorene. Sensors (Basel). 2018;18(11):3638.

[26] Furlan KP, de Mello JDB, Klein AN. Self-lubricating composites containing MoS2: a review. Tribol Int. 2018;120:280–298.

[27] Bazaka K, Levchenko I, Lim JWM, et al. MoS 2 -based nanostructures: synthesis and applications in medicine. J Phys D Appl Phys. 2019;52(18):183001.

[28] Liu T, Liu Z. 2D MoS nanostructures for biomedical applications. Adv Healthc Mater. 2018;7(8):1701158.

[29] Bhattacharya D, Mukherjee S, Mitra RK, et al. Size-dependent optical properties of MoS 2 nanoparticles and their photo-catalytic applications. Nanotechnology. 2020;31(14):145701.

[30] Arkadiusz PG, Lapinska A, Czerniak-Łosiewicz K, et al. Thermal properties of thin films made from MoS2 nanoflakes and probed via statistical optothermal Raman method. Sci Rep. 2019;13338.

[31] Taube A, Judek J, Łapińska A, et al. Temperature-dependent thermal properties of supported MoS 2 monolayers. ACS Applied Materials & Interfaces. 2015;7(9):5061–5065.

[32] Yanguang L, Wang H, Xie L, et al. MoS 2 nanoparticles grown on graphene: an advanced catalyst for the hydrogen evolution reaction. Journal of the American Chemical Society. 2011;133 (19):7296–7299.

[33] Voiry D, Salehi M, Silva R, et al. Conducting MoS2 nanosheets as catalysts for hydrogen evolution reaction. Nano Lett. 2013;13 (12):6222–6227.

[34] Tianshu L, Galli G. Electronic properties of MoS_2 nanoparticles. The Journal of Physical Chemistry C. 2007;111(44):16192–16196.

[35] Wu H, Li X, He X, et al. An investigation on the lubrication mechanism of MoS2 nanoparticles in unidirectional and reciprocating sliding point contact: the flow pattern effect around contact area. Tribol Int. 2018;122:38–45.

[36] Rajendhran N, Palanisamy S, Periyasamy P, et al. Enhancing of the tribological characteristics of the lubricant oils using Ni-promoted MoS2 nanosheets as nano-additives. Tribol Int. 2018;118:314–328.

[37] Wu P-R, Kong Y-C, Ma Z-S, et al. Preparation and tribological properties of novel zinc borate/MoS2 nanocomposites in grease. J Alloys Compd. 2018;740:823–829.

[38] Li H, Yang Q, Mo F, et al. MoS2 nanosheets with expanded interlayer spacing for rechargeable aqueous Zn-ion batteries. Energy Storage Mater. 2019;19:94–101.

[39] Yang H, Wang M, Liu X, et al. MoS2 embedded in 3D interconnected carbon nanofiber film as a free-standing anode for sodium-ion batteries. Nano Res. 2018;11(7):3844–3853.

[40] Wu J, Lu Y, Wu Z, et al. Two-dimensional molybdenum disulfide (MoS2) with gold nanoparticles for biosensing of explosives by optical spectroscopy. Sens Actuators B Chem. 2018;261:279–287.

[41] Yadav V, Roy S, Singh P, et al. 2D Mos 2 -based nanomaterials for therapeutic, bioimaging, and biosensing applications. Small. 2019;15(1):1803706.

[42] Wang F, Qu X, Liu D, et al. Upconversion nanoparticles-MoS2 nanoassembly as a fluorescent turn-on probe for bioimaging of reactive oxygen species in living cells and zebrafish. Sens Actuators B Chem. 2018;274:180–187.

[43] Hassanzadeh J, Khataee A. Ultrasensitive chemiluminescent biosensor for the detection of cholesterol based on synergetic

peroxidase-like activity of MoS2 and graphene quantum dots. Talanta. 2018;178:992–1000.
[44] Wu M-H, Li L, Xue YC, et al. Fabrication of ternary GO/g-C3N4/MoS2 flower-like heterojunctions with enhanced photocatalytic activity for water remediation. Appl Catal B Environ. 2018;228:103–112.
[45] Ma C, Ma Y, Sun Y, et al. Colorimetric determination of Hg2+ in environmental water based on the Hg2+-stimulated peroxidase mimetic activity of MoS2-Au composites. J Colloid Interface Sci. 2019;537:554–561.
[46] Yim C, O'Brien M, McEvoy N, et al. Investigation of the optical properties of MoS 2 thin films using spectroscopic ellipsometry. Appl Phys Lett. 2014;104(10):103114.
[47] Ponomarev EA, Neumann-Spallart M, Hodes G, et al. Electrochemical deposition of MoS2 thin films by reduction of tetrathiomolybdate. Thin Solid Films. 1996;280(1–2):86–89.
[48] Ling C, Ouyang Y, Shi L, et al. Template-Grown MoS 2 nanowires catalyze the hydrogen evolution reaction: ultralow kinetic barriers with high active site density. ACS Catal. 2017;7(8):5097–5102.
[49] Kumar R, Goel N, Kumar M. High performance NO 2 sensor using MoS 2 nanowires network. Appl Phys Lett. 2018;112(5):053502.
[50] Zhuo S, Xu Y, Zhao W, et al. Hierarchical nanosheet-based MoS 2 nanotubes fabricated by an anion-exchange reaction of MoO 3 -amine hybrid nanowires. Angew Chem. 2013;52(33):8602–8606.
[51] Hu KH, Wang YR, Hu XG, et al. Preparation and characterisation of ball-like MoS 2 nanoparticles. Mater Sci Technol. 2007;23(2):242–246.
[52] Zeng X, Qin W. Synthesis of MoS2 nanoparticles using MoO3 nanobelts as precursor via a PVP-assisted hydrothermal method. Mater Lett. 2016;182:347–350.
[53] Kumar KS, Li W, Choi M, et al. Synthesis and lithium storage properties of MoS2 nanoparticles prepared using supercritical ethanol. Chem Eng J. 2016;285:517–527.
[54] Liu H, Lv T, Zhu C, et al. Efficient synthesis of MoS2 nanoparticles modified TiO2 nanobelts with enhanced visible-light-driven photocatalytic activity. J Mol Catal A Chem. 2015;396:136–142.
[55] Sinha SS, Yadgarov L, Aliev SB, et al. MoS 2 and WS 2 nanotubes: synthesis, structural elucidation, and optical characterization. The Journal of Physical Chemistry C. 2021;125(11):6324–6340.
[56] Nath M, Govindaraj A, Rao CNR. Simple Synthesis of MoS2 and WS2 Nanotubes. Adv Mater. 2001;13(4):283–286.
[57] Zhong Y, Liu D, Wang L-T, et al. Controllable synthesis of hierarchical MoS_2 nanotubes with ultra-uniform and superior storage potassium properties. J Colloid Interface Sci. 2020 March 1;561:593–600.
[58] Brontvein O, Vishakantaiah Jayaram KPJR, Jeffrey MG, et al. Two-step synthesis of MoS_2 nanotubes using shock waves with lead as growth promoter. 2014;640(6):1152–1158.
[59] Chen J, Suo-Long L, Qiang X, et al. Synthesis of open-ended MoS2 nanotubes and the application as the catalyst of methanation. Chem Comm. 2002;16:1722–1723. DOI:10.1039/b205109e
[60] Remskar M, Mrzel A, Skraba Z, et al. Self-assembly of subnanometer-diameter single-wall MoS $_2$ nanotubes. Science. 2001;292(5516):479.
[61] Zelenski CM, Dorhout PK. Template synthesis of near-monodisperse 1 microscale nanofibers and nanotubules of MoS 2. J Am Chem Soc. 1998;120(4):734–742.
[62] Barreau N, Bernède JC. Low-temperature preparation of MoS2 thin films on glass substrate with NaF additive. Thin Solid Films. 2002;403-404:505–509.
[63] Yu H, Liu Y, Brock SL. Synthesis of discrete and dispersible MoS 2 nanocrystals. Inorg Chem. 2008;47(5):1428–1434.
[64] Sun Y, Wang S, Wang Q. Flowerlike MoS2 nanoparticles: solvothermal synthesis and characterization. Front Agric China. 2009;4(2):173–176.
[65] Wilcoxon JP, Newcomer PP, Samara GA. Synthesis and optical properties of MoS2 and isomorphous nanoclusters in the quantum confinement regime. J Appl Phys. 1997;81(12):7934–7944.
[66] Yang H, Zhao J, Wu C, et al. Facile synthesis of colloidal stable MoS2 nanoparticles for combined tumor therapy. Chem Eng J. 2018;351:548–558.
[67] Wang H, Li X, Yan K, et al. Low-temperature synthesis of near-monodisperse globular MoS2 nanoparticles with sulphur powders. Nano. 2017 Aug 4;12(8):1750091.
[68] Li Q, Newberg JT, Walter EC, et al. Polycrystalline molybdenum disulfide (2H–MoS 2) nano- and microribbons by electrochemical/chemical synthesis. Nano Lett. 2004;4(2):277–281.
[69] Chang K, Chen W. l -cysteine-assisted synthesis of layered MoS 2 /graphene composites with excellent electrochemical performances for lithium ion batteries. ACS Nano. 2011;5(6):4720–4728.
[70] Pourabbas B, Jamshidi B. Preparation of MoS2 nanoparticles by a modified hydrothermal method and the photo-catalytic activity of MoS2/TiO2 hybrids in photo-oxidation of phenol. Chem Eng J. 2008;138(1–3):55–62.
[71] Li Y, Cain JD, Hanson ED, et al. Au@MoS 2 core–shell heterostructures with strong light–matter interactions. Nano Lett. 2016;16(12):7696–7702.
[72] Cain JD, Shi F, Wu J, et al. Growth mechanism of transition metal dichalcogenide monolayers: the role of self-seeding fullerene nuclei. ACS Nano. 2016;10(5):5440–5445.
[73] Alinejadian N, Kollo L, Odnevall I. Progress in additive manufacturing of MoS2-based structures for energy storage applications–A review. Mater Sci Semicond Process. 2022;139:106331.
[74] Swetha C, Feaster J, Ynzunza J, et al., Three-dimensional printed MoS2/graphene aerogel electrodes for hydrogen evolution reactions. ACS Materials Au. 2022;
[75] Ghosh K, Ng S, Iffelsberger C, et al. 2D MoS2/carbon/polylactic acid filament for 3D printing: photo and electrochemical energy conversion and storage. Appl Mater Today. 2022 Mar 1;26:101301.
[76] Wang M, Li G, Xu H, et al. Enhanced lithium storage performances of hierarchical hollow MoS 2 nanoparticles assembled from nanosheets. ACS Appl Mater Interfaces. 2013;5(3):1003–1008.
[77] Jiang Y, Li X, Yu S, et al. Reduced graphene oxide-modified carbon nanotube/polyimide film supported MoS 2 nanoparticles for electrocatalytic hydrogen evolution. Adv Funct Mater. 2015;25(18):2693–2700.
[78] Hu KH, Cai YK, Hu XG, et al. Synthesis and tribological properties of MoS 2 composite nanoparticles with different morphologies. Surf Eng. 2011;27(7):544–550.
[79] Huang J, Dong Z, Li Y, et al. MoS2 nanosheet functionalized with Cu nanoparticles and its application for glucose detection. Mater Res Bull. 2013;48(11):4544–4547.
[80] Wu J-Y, Lin M-N, Wang L-D, et al. Photoluminescence of MoS_2 prepared by effective grinding-assisted sonication exfoliation. J Nanomater. 2014;2014:852735.
[81] Ho Y-T, Ma C-H, Luong -T-T, et al. Layered MoS2 grown on c -sapphire by pulsed laser deposition, physica status solidi (RRL. Rapid Res Letters. 2015;9:187–191.
[82] Dong H, Liu C, Ye H, et al. Three-dimensional nitrogen-doped graphene supported molybdenum disulfide nanoparticles as an advanced catalyst for hydrogen evolution reaction. Sci Rep. 2015;5(1):17542.
[83] Hong L, Zhang Q, Chong Ray Yap C, et al. From bulk to monolayer MoS2: evolution of raman scattering. Adv Funct Mater. 2012;22(7):1385–1390.
[84] Lianga L, Meunier V. First-principles raman spectra of MoS2, WS2 and their heterostructures. Nanoscale. 2014;10(10):5394–5401.
[85] Dumcenco D, Ovchinnikov D, Marinov K, et al. Large-area epitaxial monolayer MoS 2. ACS Nano. 2015;9(4):4611–4620. D.B.
[86] Nimbalkar -H-HL, Ramacharyulu PVRK, Ke S-C. Improved photocatalytic activity of RGO/MoS 2 nanosheets decorated on TiO 2 nanoparticles. RSC Adv. 2016;6(38):31661–31667.
[87] Ahmad R, Srivastava R, Yadav S, et al. Functionalized molybdenum disulfide nanosheets for 0D–2D hybrid nanostructures: photoinduced charge transfer and enhanced photoresponse. J Phys Chem Lett. 2017;8(8):1729–1738.
[88] Li X, Zhu H. Two-dimensional MoS2: properties, preparation, and applications. J Materiom. 2015;1(1):33–44.

[89] Li Z, Chang S-W, Chen -C-C, et al. Enhanced photocurrent and photoluminescence spectra in MoS2 under ionic liquid gating. Nano Res. 2014;7(7):973–980.
[90] Gołasa K, Grzeszczyk M, Korona K, et al. Optical properties of molybdenum disulde (MoS 2. Acta Physica Polonica A. 2013;124 (5):849.
[91] Eda G, Yamaguchi H, Voiry D, et al. Photoluminescence from chemically exfoliated MoS 2. Nano Lett. 2011;11(12):5111–5116.
[92] Guo G, Hong J, Cong C, et al. Molybdenum disulfide synthesized by hydrothermal method as anode for lithium rechargeable batteries. J Mater Sci. 2005;40(9–10):2557–2559.
[93] Hou K, Wang J, Yang Z, et al. One-pot synthesis of reduced graphene oxide/molybdenum disulfide heterostructures with intrinsic incommensurateness for enhanced lubricating properties. Carbon. 2017;115:83–94.
[94] Zhang Y, Shimeng Y, Wang H, et al. A novel carbon-decorated hollow flower-like MoS2 nanostructure wrapped with RGO for enhanced sodium-ion storage. Chem Eng J. 2018;343:180–188.
[95] Hou S, Li Y, Huo Y, et al. Preparation of nano-scale molybdenum disulfide by liquid phase precipitation method and its lubricating properties. Ferroelectrics. 2018;524(1):79–85.
[96] Hu KH, Hu XG, Xu YF, et al. The effect of morphology on the tribological properties of MoS2 in liquid paraffin. Tribology Lett. 2010;40(1):155–165.
[97] Prabhakar Vattikuti SV, Byon C, Venkata Reddy C, et al. Synthesis and structural characterization of MoS2 nanospheres and nanosheets using solvothermal method. J Mater Sci. 2015;50 (14):5024–5038.
[98] Kogovšek J, Kalin M. Various MoS2-, WS2- and C-based micro- and nanoparticles in boundary lubrication. Tribology Lett. 2014;53 (3):585–597.
[99] Yi M, Zhang C. The synthesis of MoS2 particles with different morphologies for tribological applications. Tribol Int. 2017;116:285–294.
[100] Winer WO. Molybdenum disulfide as a lubricant: a review of the fundamental knowledge. Wear. 1967;10(6):422–452.
[101] Stephenson T, Li Z, Olsen B, et al. Lithium ion battery applications of molybdenum disulfide (MoS 2) nanocomposites. Energy Environ Sci. 2014;7(1):209–231.
[102] Arul NS, Nithya VD. Molybdenum disulfide quantum dots: synthesis and applications. RSC Adv. 2016;6(70):65670–65682.
[103] Azhagurajan M, Kajita T, Itoh T, et al. In situ visualization of lithium ion intercalation into MoS2 single crystals using differential optical microscopy with atomic layer resolution. J Am Chem Soc. 2016;138(10):3355–3361.
[104] Chang K, Chen W, Ma L, et al. Graphene-like MoS 2/amorphous carbon composites with high capacity and excellent stability as anode materials for lithium ion batteries. J Mater Chem. 2011;21 (17):6251–6257.
[105] Wang S, Li G, Du G, et al. Hydrothermal synthesis of molybdenum disulfide for lithium ion battery applications. Chin J Chem Eng. 2010;18(6):910–913.
[106] Gupta U, Rao CNR. Hydrogen generation by water splitting using MoS2 and other transition metal dichalcogenides. Nano Energy. 2017;41:49–65.
[107] Liu Y, Yu Y-X, Zhang W-D. MoS 2 /CdS heterojunction with high photoelectrochemical activity for H 2 evolution under visible light: the role of MoS 2. J Phys Chem C. 2013;117 (25):12949–12957.
[108] Wang Z, Mi B. Environmental applications of 2D molybdenum disulfide (MoS 2) nanosheets. Environ Sci Technol. 2017;51 (15):8229–8244.
[109] Sarkar D, Liu W, Xie X, et al. MoS 2 field-effect transistor for next-generation label-free biosensors. ACS Nano. 2014;8 (4):3992–4003.
[110] Lee K, Gatensby R, McEvoy N, et al. High-performance sensors based on molybdenum disulfide thin films. Adv Mater. 2013;25 (46):6699–6702.
[111] Li H, Yin Z, He Q, et al. Fabrication of single- and multilayer MoS2 film-based field-effect transistors for sensing NO at room temperature. Small. 2012;8(1):63–67.
[112] Zhang S-L, Choi -H-H, Yue H-Y, et al. Controlled exfoliation of molybdenum disulfide for developing thin film humidity sensor. Curr Appl Phys. 2014;14(3):264–268.
[113] Chao Y, Zhu W, Wu X, et al. Application of graphene-like layered molybdenum disulfide and its excellent adsorption behavior for doxycycline antibiotic. Chem Eng J. 2014;243:60–67.
[114] Liu Q, Hu C, Wang X. A facile one-step method to produce MoS 2 quantum dots as promising bio-imaging materials. RSC Adv. 2016;6(30):25605–25610.
[115] Yin W, Liu X, Zhang X, et al. Synthesis of tungsten disulfide and molybdenum disulfide quantum dots and their applications. Chem Mater. 2020;32(11):4409–4424.
[116] Jaiswal K, Girish YR, Behera P, et al. Dual role of MoS 2 quantum dots in a cross-dehydrogenative coupling reaction. ACS Organic Inorg Au. 2022;2(3):205–213.
[117] Liu C, Jia F, Wang Q, et al. Two-dimensional molybdenum disulfide as adsorbent for high-efficient Pb(II) removal from water. Appl Mater Today. 2017;9:220–228.
[118] Song HJ, You S, Jia XH, et al. MoS2 nanosheets decorated with magnetic Fe3O4 nanoparticles and their ultrafast adsorption for wastewater treatment. Ceram Int. 2015;41 (10):13896–13902.
[119] Massey AT, Gusain R, Kumari S, et al. Hierarchical microspheres of MoS 2 nanosheets: efficient and regenerative adsorbent for removal of water-soluble dyes. Ind Eng Chem Res. 2016;55(26):7124–7131.